Spring thermal bar dynamics and impacts on plankton biomass and composition in southeast Lake Michigan

by

Yifan Zhang

A thesis submitted

in partial fulfillment of the requirements

for the degree of

Master of Science

(Environment and Sustainability)

in the University of Michigan

April 2021

Thesis Committee:

Dr. Sara Adlerstein Gonzalez, Chair

Dr. Edward Rutherford

Abstract

This study identified formation time, movement and disappearance of spring thermal bars in southeast Lake Michigan off Muskegon from 2010 to 2019, and analyzed 2019 and 2015 zooplankton distribution and composition in response to thermal bar dynamics and environmental characteristics. Thermal bar location was identified using available Sea Surface Temperature satellite data. Analysis of zooplankton biomass and composition distribution with environmental characteristics used data from NOAA and Great Lakes Environmental Laboratories research programs. Analysis used generalized linear models. Results showed that thermal bars formed mainly in April, persisted one to four weeks, and formation and movements influenced by air temperature occurred later with cooler air. Location relative to shore was positive and significantly influenced by runoff and air temperature 7 days prior to the thermal bar identification, but not significantly influenced by air temperature on the day bars were identified. Movement rate towards offshore, ranging 0 to 3.53 cm/s, increased significantly with air temperature 10 days prior to the end of thermal bar movements and with distance to shore but was not significantly related to river runoff discharge. Zooplankton biomass significantly varied among zones relative to thermal bars along the Muskegon transect and was higher in zones inshore from thermal bars. Chlorophyll a (CHL) biomass was highest nearshore from thermal bars with highest colored dissolved organic matter (CDOM) and water temperature. Zooplankton biomass distribution was consistent with CHL, water temperature and CDOM distribution. Zooplankton composition also varied among areas relative to thermal bars. In 2015, *Leptodiaptomus sicilis* copepod was most abundant in nearshore areas in April and near thermal bars with preferred cooler temperatures in May. In 2019, *L. sicilis* and *L. ashlandi* were most abundant near thermal bars in April, but decreased in May as cyclopoid copepod *Diacyclops thomasi* became more abundant.

Acknowledgements

Foremost, I would like to express my sincere gratitude to my advisor Dr. Sara Adlerstein Gonzalez and co-advisor Dr. Ed Rutherford for their guidance, patience and continued support of my research and thesis writing. I would also like to thank them for their encouragement and care during this special year with Covid-19, and thank them for every pleasant meeting.

I would like to express my appreciation to NOAA GLERL for survey data on water quality and plankton biomass. In particular, the GLERLs long-term research program led by Steven Pothoven provided zooplankton net data in 2015, and Henry Vanderploeg's Spatial Studies program provided 2015 and 2019 PSS data and zooplankton data. Thank you, David Wells, who trained me on species identification of larval fish. Thank you, Dr. Paul Seelbach, who helped me borrow equipment from the laboratory. Finally, I would like to thank Kuiran Zhang, who always gave me great support and encouragement.

Table of Contents

1 Introduction

1.1 Thermal bar definition

Thermal bars are temperature fronts that form annually in lakes in spring and autumn (Holland and Kay, 2003) due to preferential warming (in spring) or cooling (in fall) of shallow nearshore waters (Ullman et al, 1998). This study only focused on the spring thermal bar and all thermal bars mentioned below are spring thermal bars. When water reaches its maximum density at 4 ℃, the water sinks to form a vertical front that separates the lake into warmer inshore （>4℃） and colder offshore water （<4℃） (Stoermer, 1968; Bukreev and Gavrilov, 2010). Thermal bars act as boundaries between water bodies that control the mixing of nearshore and offshore waters and limit the exchange of heat and mass (Huang, 1972; Blanton, 1986; Lathrop et al, 1990). Thermal bars play an important role in the ecosystem because high primary productivity often occurs within thermal bars, which impact the distribution, composition and production of zooplankton and fish through the food web (Mortimer, 1988; Moll et al, 1993). Information about timing and location of the thermal bar can be valuable for predicting biological processes in lakes.

1.2 Impact of thermal bars on nutrient cycles

Thermal bars are important in regulating physical, chemical and biological processes. They impact the distribution of sediments, nutrients and organisms, through hydrodynamics. For example, in Lake Superior, average nearshore total suspended sediment (TSS) levels can be raised more than four times background levels due to nutrients and sediments delivered during spring runoff events that are trapped by the thermal bar (Auer and Gatzke, 2004). Further, the date of the thermal bar formation relative to runoff events determines the proportion of total suspended sediment from spring runoff events trapped in the nearshore waters.

1.3 Impact of thermal bars on plankton distribution

During spring, there are two abundant plankton areas in lakes with distinct regimes: the nearshore area with high production and the area near the thermal bar due to convergent zones (Holland and Kay, 2003).

1.3.1 Nearshore area

Studies in Lake Baikal and Lake Michigan have documented that spring growth of phytoplankton and zooplankton is faster inshore of the thermal bar due to more suitable temperatures and higher nutrient levels compared to areas outside of the thermal bar (Saiz et al, 1992; Tsydenov, 2019; Wang, 2013; Vanderploeg et al, 2007; Moll et al, 1993). Additionally, more stable flow inside of the thermal bar benefits the growth of phytoplankton and zooplankton.

Primary productivity in lakes increases during spring blooms because of enhanced

insolation and relatively high nutrient levels that provide optimal conditions for phytoplankton growth (Holland and Kay, 2003; Ullman et al, 1998). Injection of algae from river runoff into the nearshore regions may serve as a "seed" population for phytoplankton blooms immediately inshore of the thermal bar (Bowers et al, 1986). In Lake Baikal, temperature is the dominant reason for higher zooplankton abundance in nearshore areas (Tsydenov, 2019). In early stages of thermal bar development, growth of phytoplankton and zooplankton biomass is observed in the nearshore area of the lake. Nevertheless, when the thermal bar moves offshore, highest zooplankton concentrations remain in the nearshore area due to warmer water conditions while highest phytoplankton concentrations may occur offshore but near the thermal bar in Lake Bailkai (Tsydenov, 2019). Additionally, thermal bars can have an effect on environmental stability for plankton growth in open water, which has been emphasized in ecological studies in Kootenay Lake and Lake Michigan (Jasper et al, 1983; Scavia and Fahnenstiel, 1987). Continued growth of plankton is allowed when biomass is kept within the euphotic zone due to restriction of vertical mixing.

1.3.2 Convergence zone

Aggregation of plankton and planktonic organisms at the thermal bar has been explained by passive accumulation at convergence zones and by in situ production (Owen, 1981). In Lake Ontario, phytoplankton blooms confined nearshore by the thermal bar at first migrate offshore when the thermal bar moves due to the effects of convergence (Scavia and Bennett, 1980). In addition, convergent flow may move phytoplankton and zooplankton towards the thermal bar and below the surface. The convergence and downwelling can rapidly move phytoplankton and zooplankton from the surface to the bottom where they may serve as an important source of food for the benthos (Moll et al, 1993).

1.4 Impact of thermal bars on fish survival, growth and distribution in Lake Michigan

Regions inshore of thermal bars may provide suitable habitat for growth and survival of larval fish because of enhanced densities of prey and favorable temperatures. In Lake Michigan, higher density of larval deepwater sculpin was found inshore of the thermal bar compared to offshore (Wang, 2013). Additionally, larvae inshore of the thermal bar were found to have higher growth rates and to consume significantly ($p < 0.04$) more copepod prey than larvae offshore. Higher consumption and growth rates could result in larger body sizes of larvae, and a better ability to catch prey and avoid predators (Miller et al, 1988, 1992). While fish eggs and larvae passively accumulate at thermal bars, adult fish that are capable of overcoming physical advection also are often observed aggregated at the thermal bar owing to increased food availability and better thermal conditions in Lake Michigan (Brandt et al,1980; Brandt and Wadley, 1981).

1.5 Bottom-up effects in Lake Michigan

Phytoplankton blooms have declined in nearshore and offshore areas of Lake

Michigan since 1970 (Madenjian et al, 2002, Fahnenstiel et al, 2016). This has led to changes in phytoplankton and zooplankton density and composition, which ultimately affect fish populations through bottom-up effects. Annual primary production in the offshore waters of Lake Michigan has been estimated to have decreased by 35% between 1983–1987 and 2007–2008, attributed to the filtering activities of quagga mussels during spring mixing (Fahnenstiel et al, 2010; Vanderploeg et al, 2010). This change also occurred in nearshore areas, and reduction in primary production may have partly contributed to the decrease in Diporeia abundance in the nearshore region during the early 1990s (Nalepa et al, 2000). These bottom-up effects have already influenced populations of some fish species. For example, the decrease in lake whitefish populations between 1995 and 1998 may have been partially due to bottom-up effects (Madenjian et al, 2002).

1.6 Studies are needed on thermal bar dynamics in Lake Michigan

Several studies have reported that timing of thermal bar formation in the Great Lakes is primarily determined by latitude, water depth, climatic conditions and river runoff (Auer and Gatzke, 2004; MaIm and Jonsson, 1993; Spain et al, 1976; Blokhina, 2015; Tsydenov, 2019). Ullman et al (1998) estimated the temporal probability of thermal bars occurring in different Great Lakes regions through the application of an edge-detecting algorithm (Cayula and Cornillon, 1992) to sea surface temperature (SST) images. This study estimated that the spring thermal bar appears earliest in shallow Lake Erie and latest in Lake Superior, the deepest and northernmost of the lakes. Further, in Lakes Michigan and Huron, the thermal bar is estimated to appear later in northern than in southern waters because these lakes span large latitudinal ranges. During 1985-1995, in Lake Michigan, the thermal bar reached its peak during May and weakened in June (Ullman et al, 1998). In July, it disappeared in the south but still was identified in the northeast. Auer and Gatzke (2004) documented the date of formation of the thermal bar in Lake Superior during a 33-year period (1966–1998) to range from 6 April (1969) to 28 May (1972), with an average date of 2 May (± 13 days). To some degree, this variability is due to meteorological conditions.

The speed of the spring thermal bar movement in the Great Lakes and other lakes is thought to depend on the heating rate, bottom slope, late winter lake temperature and wind (MaIm and Jonsson, 1993; Spain et al, 1976; Blokhina, 2015; Tsydenov, 2019). According to Scavia and Bennett (1980), the spring thermal bar progresses from shore to the center of Lake Ontario at a rate of 0.5-1.0 cm/s. According to Elliott (1970), model predicted thermal bar speeds for Lake Ontario were 0.3 cm/s and 0.95 cm/s at the south and north shore respectively. Warming from solar insolation and river runoff are considered to be basic thermal regimes that set the speed of the thermal bar movement (Bennett, 1971; Rodgers, 1987). Furthermore, wind plays an important role in the lake hydrodynamics during the thermal bar period (Blokhina, 2015). Winds opposite to the direction of the thermal bar can slow its horizontal movement (Tsydenov, 2019). In addition, thermal bar movement speed is predicted to vary inversely with the lake bottom slope such that in steep areas, a higher proportion of water at the lake bottom seems to flow offshore. The entry of offshore

water into inshore areas contributes to the thermal bar movement so the thermal bar speed is slower in steep areas (MaIm and Jonsson, 1993; Spain et al, 1976).

Although available studies have described the basic regime of thermal bar formation, movement, timing, and speed, dominant impacts still need to be explored. In this study, I aim to describe the processes of thermal bar formation, movement, and disappearance in southeast Lake Michigan between 2010 and 2019, and identify the influence of air temperature, runoff temperature, runoff discharge and distance to shore on the thermal bar dynamics.

1.7 Studies are lacking of the interaction of thermal bar dynamics with zooplankton biomass and composition in Lake Michigan

Few studies have explored differences in zooplankton biomass and species composition relative to thermal bar location in Lake Michigan (Wang, 2013; Pothoven and Fahnenstiel, 2015; Agy, 2001). Although these studies have demonstrated that zooplankton biomass is higher inshore due to in situ production or physical accumulation, not all zooplankton species aggregate there. For example, in a study of the thermal bar off Lake Michigan's western shore, the density of Limnocalanus copepods did not significantly differ between inshore and offshore of the thermal bar (Wang, 2013).

Some studies in Lake Michigan have compared zooplankton composition and biomass among nearshore, mid-depth and offshore areas. Pothoven and Fahnenstiel (2015) found that during 2007–2012, differences in zooplankton species composition in southeastern Lake Michigan intensified from spring into summer, but weakened in the fall. Pothoven and Fahnenstiel (2015) and Agy (2001) found that copepods in offshore areas were larger than in nearshore areas, especially in summer. Small-bodied diaptomids (*Limnocalanus minutus*) constituted a higher percentage of the total copepod biomass at nearshore sites while large bodied diaptomids (*L. sicilis*) constituted a higher percentage of total biomass at mid-depth and offshore sites. While zooplankton bathymetric and seasonal composition in Lake Michigan has been studied, variation in zooplankton size and species composition relative to thermal bars has not been explored. Biomass and size of zooplankton between nearshore and offshore areas are known to change depending on season. In the nearshore, peak biomass of zooplankton is observed during early summer and is related to rapid and early warming of water temperature, whereas at mid-depth and offshore areas, the peak zooplankton biomass is found in late summer (Dettmers et al, 2003). In spring, water inside of the thermal bar has higher concentrations of phytoplankton and is expected to foster zooplankton growth (Brandt, 2013). However, in summer, size selective fish predation has been found to be larger in nearshore areas, causing the sizes of zooplankton to be smaller in nearshore habitats compared to offshore (Evans, 1990; Agy, 2001).

I hypothesized that: i) runoff discharge, air temperature and distance to shore have a significant effect on thermal bar speed, ii) zooplankton biomass is higher in areas

inshore of the thermal bar compared to areas offshore due to the trapping effects of chlorophyll a (CHL) by thermal bars and iii) that CHL biomass is higher inshore than offshore due to the trapping effects of CDOM, nutrients and chlorophyll by thermal bars.

2 Objectives

The objectives of this study are to: (1) describe the timing of formation, movement and disappearance of the thermal bar in southeast Lake Michigan in the last decade; (2) investigate the effects of air temperature, runoff temperature, runoff discharge and distance to shore on the thermal bar dynamics including thermal bar distance to shore and speed; (3) explore variation in zooplankton biomass, species and size composition in relation to variation in environmental characteristics around the thermal bar.

3 Study Area

The study area is in southeast Lake Michigan off Muskegon (Figure 1). The slope of the nearshore area (0-30 m depth) is gentle, but in parts of the mid-depth region (30-60 m) increases sharply from 45 to 100 m before leveling off from 100 to 110 m (Figure 2). The distance from shore to a depth of 45 m is 10.5 km, while the distance from 45 to 100 m depth offshore increases by only 5.2 km. In spring, the study area is characterized by a gradient of decreasing temperature and nutrients from nearshore to offshore due to warm, nutrient rich tributary runoff from the Muskegon River and Grand River (Auer and Gatzke, 2004; Moll et al, 1993).

Spring phytoplankton blooms in the nearshore area off Muskegon have total chlorophyll concentrations reaching up to 7.0 μg L^{-1}, several times greater than concentrations offshore (1.7 μg L^{-1}) (Carrick et al, 2015). Further, during spring offshore areas are dominated by picoplankton (< 2 μm) and nearshore areas by nano- (2-20 μm) and micro-plankton (> 20 μm). During July, after water is vertically stratified, both the total chlorophyll concentration and phytoplankton size distribution are more similar in nearshore and offshore areas (Carrick et al, 2015).

The study area in southeast Lake Michigan was selected because of the availability of several sources of data, in particular data collected along a transect off Muskegon between latitude 43.188N-43.206N and longitude 86.33W-86.64W (Figure 1) from an ongoing long-term ecological research study by NOAAs Great Lakes Environmental Research Laboratory (GLERL).

4 Material and Methods

Data for this study were obtained from databases generated by projects conducted

by the NOAA Great Lakes Environmental Research Laboratory (NOAA GLERL) and the United States Geological Survey (USGS). These projects include: i) NOAA CoastWatch; ii) USGS National Water Information System; iii) NOAA GLERLs Real-Time Meteorological Observation Network (RECON); iv) NOAA GLERLs Plankton Survey System (PSS); and v) NOAA GLERLs long-term research program on lower trophic levels of Lake Michigan (Table 1).

4.1 Data sources

4.1.1 NOAA CoastWatch water temperature data

To describe the timing of formation, disappearance and speed of the spring thermal bar, I analyzed High-resolution Sea Surface Temperatures (SST) estimated from Advanced Very High Resolution Radiometer (AVHRR) infrared satellite data for Lake Michigan obtained from the ERDDAP (Environmental Research Division's Data Access Program) Server (https://coastwatch.noaa.gov/erddap/index.html). Separate datasets with 3-days, 7-days and monthly resolution are available. To identify the thermal bar location, I used the 3-days resolution dataset and when data were limited, I used the 7-days resolution dataset. Measurements are made from NOAA Polar Operational Environmental Satellites (POES) and the European MetOp Satellites conducted by CoastWatch. SST is measured using AVHRR's infrared (IR) channels. The radiance measured is converted to brightness temperature and a multichannel technique is used to calculate SST.

SST data are available in the form of satellite images and tables with corresponding Universal Coordinated Time of collection, location and surface temperature in degrees centigrade (℃) associated with each image pixel. Images are composed of pixels covering part of or the entire Muskegon transect (Figure 3). The approximate resolution of the pixels is 1.02 km for latitude and 0.76 km for longitude. The area of the Muskegon transect is covered by two rows of pixels along latitudes 43.194N and 43.204N and 34 pixels between 86.33W and 86.64W, about 25 km. On some dates, data covering a portion of the transect were not available to search for the thermal bar location because the coverage range of AVHRR was limited by clouds. Mean bias errors for AVHRR data (AVHRR - buoy) were estimated to range from +0.44°C to +0.51°C for three NOAA POES satellites (Ullman et al 1998).

4.1.2 USGS National Water Information System and NOAA GLERL Real-Time Meteorological Observation Network meteorological data

To investigate effects of meteorological factors on the thermal bar speed, I used data on water temperature and discharge of the Muskegon River runoff near Croton dam (https://nwis.waterdata.usgs.gov/nwis). Data were obtained by the Grayling Field office and measured by on-site automated recording equipment at 15 min intervals. To verify accuracy, streamflow and gage height were manually measured as a supplement. Air temperatures at Muskegon, monitored by the NOAA Real-Time Meteorological Observation Network, and average daily air temperatures were obtained at https://www.glerl.noaa.gov/metdata/mkg/archive/.

4.1.3 NOAA GLERL Plankton Survey System (PSS) data

To investigate effects of the thermal bar on zooplankton biomass, chlorophyll a (CHL) biomass, light (PAR, or photosynthetic active radiation), temperature, nutrient level (CDOM, or colored dissolved organic matter), I analyzed data collected by the PSS. The PSS survey is described by Vanderploeg et al (2007), when it was deployed along five transects in southern Lake Michigan including the one off Muskegon shown in Figure 1. I used the PSS data sampled monthly along the Muskegon transect in April and May of 2015 and 2019, and used the temperature data to identify the thermal bar. Cruises were conducted along the Muskegon transect between 86.33W - 43.188N and 86.64W - 43.207N, about 25 km. The system consists of a laser optical plankton counter (OPC) (Model 2T, Focal Technologies, Dartmouth, NS), a General Oceanics flowmeter, an Aquatracka III fluorometer (which has 4 decade logarithmic amplifiers, Chelsea Technology Group, Surrey, UK), a Biospherical Instruments PAR sensor (San Diego, CA), and an OS200 CTD (San Diego, Ocean Sciences, CA) mounted on a V-fin (Ruberg et al, 2001). The PSS is towed in a vertically undulating mode and continuously raised or lowered at 0.25 m/s between 1- 2 m from bottom to surface to create a sinusoidal path along transects as the ship moved at 2.5 m/s offshore (Figure 2).

The PSS data are geo-referenced to include time and depth. Data are recorded at 0.5s intervals (Ruberg et al, 2001). The PSS maps out continuous measures of chlorophyll, temperature PAR and CDOM (Figure 4), and zooplankton biomass (Figure 4 and Figure 5). Zooplankton are counted and biomass measured using an optical plankton counter (OPC) within five size categories (bin1 = 91-255 µm; bin2= 256-495 µm; bin3= 496-750 µm; bin4= 751-1500 µm; and bin5= 1501-4005 µm).

4.1.4 NOAA GLERLs long term research (LTR) program zooplankton data

To investigate effects of the thermal bar on zooplankton, data also were obtained from the NOAA GLERL long term research program and Plankton Survey System described by Vanderploeg et al (2007). Net tow samples of zooplankton were collected at stations along the Muskegon transect at 15m, 45m and 110m depth by LTR (Figure 1) and at 10m, 15m, 30m, 35m, 45m and 110m depth by PSS (Table 2). Two replicate tows were taken at each station using a 0.5 m diameter zooplankton net with a 64 or 153 µm mesh and vertically hauled from 1 to 2 m above the bottom to the surface. Additionally, secchi depth (measure of water clarity) and CHL biomass were measured at stations along the Muskegon transect at 15m, 45m and 110m depth by LTR.

I used data from net tow samples collected with 64-µm and 153-µm mesh nets from March to June along the Muskegon transect in 2015 and 2019 by the LTR and PSS programs (Table 2). Methodology for analysis of the samples is described by Agy (2001) and Vanderploeg et al (2012). Zooplankton samples were narcotized with Alka-Seltzer and preserved in 2–4% sugar formalin solution (Haney and Hall, 1973). Subsamples of zooplankton were taken using a Hensen-Stempel pipette from a well-mixed total sample of 500 ml. Subsamples of zooplankton were counted in a circular counting dish using a dissecting microscope at a magnification of 20 to 57 x until a

minimum of 600 zooplankton organisms were identified for each sample. Using the keys of Wilson and Yeatman (1959), Brooks (1959) and Balcer et al (1984), all adult copepods and cladocerans were classified to species, immature copepodites to genus, and nauplii combined into one group. Densities of zooplankton from subsamples were calculated on a volumetric basis. To estimate zooplankton biomass, length measurements were made on a subsample (10 adult copepods and 25 copepods or cladocerans) which were over 10% of the total density, using Image Pro Plus image analysis software (Media Cybernetics, Silver Spring, MD). Dry biomass was determined using published length-weight regressions (Culver et al, 1985; Malley et al, 1989). A default weight from the literature was used to estimate biomass for unmeasured zooplankton taxa that were less than 10% of the total density (Hawkins and Evans, 1979).

4.2 Data analysis

4.2.1 Thermal bar Identification

To address the study objectives 1 and 2 related to the thermal bar dynamics, I used 2010 to 2019 SST data to identify the location of the thermal bar along the Muskegon transect in southeast Lake Michigan (Figure 1). To identify the location, I followed the criteria that areas inshore of the thermal bar have SST ≥ 4 ℃ and areas offshore of the thermal bar have SST < 4℃. Because thermal bars are a boundary between cold < 4 ℃ and warm water > 4 ℃, I looked along the 43.194N longitude of the Muskegon transect for two adjacent pixels where SST ≥ 4 ℃ and < 4 ℃. If the pixel SST = 4 ± 0.5℃, I used coordinates of the pixel with SST closest to 4 ℃ as the thermal bar location. If no pixels were found with SST = 4 ± 0.5 ℃, I looked for two adjacent pixels with SST = 4 ± 1 ℃ and considered the location to be in the middle of the two pixels. If I found no thermal bar from pixel data along the Muskegon transect at 43.194N, I searched along pixels at longitude 43.204N.

I considered the date of thermal bar formation to be the first time I could identify it based on the above criteria. The date of disappearance was the last time it was identified before the lake reached full vertical thermal stratification. The change in location of the thermal bar between two adjacent dates was identified as a movement. If the identification of the thermal bar along the transect was uncertain due to lack of data during the six days before its first identification or six days after its last identification, I could not confirm the exact date of its formation or disappearance.

Additionally, I estimated the distance to shore of thermal bars along the Muskegon transect at water surface and lake bottom using PSS water temperature data. I identified these as the distance to shore of the surface 4 ℃ isotherm and lake bottom 4 ℃ isotherm. I looked at the trajectory of measurement points along the transect: if there were temperatures = 4 ℃± 0.5 within 5 m below the water surface or above the lake bottom, I used the location of the measurement point closest to 4°C as the thermal bar location at water surface or lake bottom. Otherwise, I looked for the measurement points on either side of the 4 ℃ isotherm with water temperature closest to 4℃ within 5 m below the water surface or above the lake bottom and

calculated the distance to the shore of the thermal bar by averaging these two measurement point distances. I also calculated the distance to shore differences between surface and lake bottom 4 ℃ isotherm.

4.2.2 Thermal bar dynamics analysis

I used Generalized Linear Models (GLMs) (McCullagh and Nelder, 1989) to evaluate the effect of: i) air temperature, ii) runoff temperature, and iii) average air temperature during the previous 7 days on the thermal bar location relative to shore the first time it was identified. Because air temperature during the previous 7 days was highly correlated with air and runoff temperature, I ran separate GLMs. I assumed a normal probability function to represent the distribution of the thermal bar distance to shore. Tests were performed at the 90% confidence level. The GLM analyses were implemented using the glm () function in R (R Core Team, 2013).

To evaluate the influence on the thermal bar speed of i) air temperature, ii) runoff discharge and iii) distance to shore, I used GLMs (McCullagh and Nelder, 1989) and considered lag effects of temperature and discharge on the thermal bar given its location. I calculated speed based on the distance and time between thermal bar locations. For each movement, I calculated air temperature as the average temperature during the 10 days prior to the end of the movement. The difference in time lag was to account for water temperature in the Muskegon River being highly correlated with the average air temperature in the previous 10 days. The lag time effect for the runoff discharge was different for movements nearshore and offshore, where the midpoint of the movement < 10.53 km or the 45 m depth contour > determined if it was considered to be nearshore or offshore. I calculated the average daily discharge at the Muskegon River 3 days prior to the movement for nearshore areas and 7 days for offshore areas. The lag time for nearshore locations is to account for about two days for runoff to move from the discharge monitoring station in the Muskegon River to nearshore areas and 7 days to reach offshore areas. Distance to shore was calculated as the distance to shore of the movement midpoint, where the shoreline is 86.32W. Distance was calculated as the difference between longitude of the thermal bar midpoint and the shoreline where 1 degree of longitude = 81km.

Average daily air temperature 7 days prior movement was highly positively correlated with distance to shore of the thermal bar. I ran two separate GLMs: one with thermal bar movement speed as a function of air temperature and runoff discharge, and another with thermal bar speed as function of distance to shore. I assumed the variation in thermal bar speed was normally distributed. Tests were performed at the 90% confidence level. The GLM analyses were implemented using the glm () function in R (R Core Team, 2013).

4.2.3 Zooplankton total biomass analysis

To analyze the effects of the thermal bar on zooplankton biomass distribution along the Muskegon transect, I used data collected in 2015 and 2019 by the GLERL PSS. Zooplankton organisms in the surveys are enumerated in five size diameter categories (bin 1 = 91-255 μm; bin 2 = 256-495 μm; bin 3 = 496-750 μm; bin 4 = 751-1500 μm;

and bin 5 = 1501-4005 µm). I compared the total biomass along the transect within four zones: Zone 1 is inshore and > 405m from the thermal bar; Zone 2 is inshore and within 405m of the thermal bar; Zone 3 is offshore and within 405m of the thermal bar; and Zone 4 is offshore and > 405 m from the thermal bar. I modelled differences in zooplankton biomass along the transect zones using GLMs (McCullagh and Nelder, 1989). I ran separate models for April and May in 2015 and 2019. I used a gamma distribution to represent the skewed biomass distribution, and a logarithmic link to implement the analysis.

4.2.4 Species composition of zooplankton biomass

To analyze the effects of the thermal bar on species composition of zooplankton biomass, I used net tow data collected in 64-µm or 153-µm mesh nets along the Muskegon transect in 2015 and 2019 by the NOAA GLERL LTR and PSS programs (Table 1). I focused on the spatial distribution of the nine most abundant zooplankton taxa in relation to the thermal bar: copepod nauplii, Diaptomid copepodites (C1-C5 stages), *Diacyclops thomasi, Leptodiaptomus ashlandi, L. minutus, L. sicilis, Limnocalanus macrurus, Bosmina longirostris* and invasive Dreissena mussel veligers. I calculated the biomass proportion of zooplankton taxa for each sample available, and compared proportions across transect zones and sample dates. These samples were collected during research cruises when the thermal bar was present in 2015 on April 28 and May 20, and in 2019 from April 29-May 2 and May 14-16. Additionally, I investigated the zooplankton biomass composition by size categories in the four transect zones using the bin1-bin5 sized zooplankton biomass estimated by the PSS laser optical plankton counter. To explore whether the zooplankton biomass composition distribution was consistent with the zooplankton size distribution, I combined the size categories of zooplankton taxa based on optical plankton counter (OPC) equivalent spherical diameters (ESD) using length and length/width ratios (Liebig and Vanderploeg, 2008) (Table 3).

Finally, to explore the effect of thermal bars on environmental factors that may influence zooplankton biomass, I calculated the average CHLbiomass, PAR, water temperature and colored dissolved organic matter (CDOM) recorded by the PSS in the four thermal bar zones along the Muskegon transect during April and May of 2015 and 2019.

5 Results

5.1 Thermal bar temporal dynamics

The thermal bar formation occurred earlier in years with higher average air and runoff temperatures in spring (Table 4) (Figure 6), but was not influenced by the average runoff discharge during this period (Figure 7). The thermal bar formation ranged from March 14 (2012) to April 28 (2015) and its disappearance ranged from April 1 (2012) to May 29 (2014). Thermal bars formed in April in most years. The exact formation in 2014 could not be determined because the first time that the bar was identified was

after three SST sampling dates during which the entire transect area or a large portion was covered by clouds (May 8, 11 and 14).

5.2 Thermal bar location relative to shore

Thermal bars for the study period were identified within 86.356W and 86.6W longitude along the Muskegon transect. Thermal bars were first observed at a distance to shore ranging from 2.9 km (2016) to 7.5 km (2011). Thermal bars were last observed at 9.8 km (2015) to 22.7 km (2013) (Figure 8). The thermal bar typically moved offshore, but was also found to regress (May 17 to 20 during 2015 and May 5 to 8 during 2019).

Model results indicated that the thermal bar distance to shore along the Muskegon transect was positively and significantly related to runoff temperature and average air temperature 7 days prior to the thermal bar identification (Table 5). There was no significant effect of air temperature on the day thermal bar was identified on the thermal bar location.

5.3 Thermal bar speed

The annual average thermal bar speed ranged from 0.5 cm/s (2015) to 1.6 cm/s (2017) with an average speed of 0.93 cm/s. Among the 31 movements identified over the 10-year period, the thermal bar speed ranged from 0 to 3.5 cm/s. Results from a GLM of thermal bar speed with covariates air temperature and runoff discharge as predictors show that speed increased significantly with air temperature but not with river discharge (Table 6) (Figure 9). Results from a GLM of the thermal bar speed as a function of distance to shore indicated that speed increased significantly with distance to shore.

5.4 Zooplankton biomass distribution around the thermal bar

Results of GLMs for 2015 and 2019 indicated that zooplankton biomass varied significantly among thermal bar zones (Figures 10 and Figure 11) and generally supported the hypothesis that zooplankton biomass was higher in zones inshore of the thermal bar than zones offshore of the thermal bar. In April and May 2015, and in May 2019, zooplankton biomass was higher in areas inshore of the thermal bar (Zones 1 and 2) than in areas offshore of the thermal bar (Zones 3 and 4). Zooplankton biomass was highest in Zone 1 in April and May in 2015 and in Zone 2 in May 2019 (Table 7). In April 2019, zooplankton biomass was higher in Zone 3 than in Zone 1 and Zone 2, but the *average* zooplankton biomass in areas inshore of the thermal bar was still higher than areas offshore of the thermal bar. In both 2015 and 2019, the lowest zooplankton biomass in April was in Zone 4, offshore of the thermal bar.

5.5 Zooplankton species composition around the thermal bar

The species composition of zooplankton biomass varied temporally and spatially around the spring thermal bar. In 2015, *Leptodiaptomus sicilis*, *L. ashlandi*, *L. minutus*, copepod nauplii and Diaptomid copepodite stages C1-C5 were the dominant species

which accounted for more than 10% of zooplankton biomass in samples when thermal bars were present in April and May. In late April 2015, zooplankton biomass in Zone 2 was mainly composed of *L. sicilis* (58.8%), *L. ashlandi* (15.7%) and *L. minutus* (15.9%) (Figure 12). Zooplankton taxa in Zone 4 were dominated by *L. sicilis* (36.1%) and *L. ashlandi* (26.1%). In May 2015, biomass in Zone 1 was mainly composed of copepod nauplii (32.5%), Diaptomid copepodite stages (C1-C5) (23.7%) and *L. minutus* (12.8%) (Figure 12). In Zone 4, zooplankton biomass was dominated by *L. sicilis* (39.0%), *L. ashlandi* (20.1%) and Diaptomid copepodite stages (C1-C5) (15.1%) (Figure 12).

In 2019, as in 2015 zooplankton biomass dominant taxa included Leptodiaptomid copepods and cyclopoid copepod Diacyclops thomasi. In late April, biomass in Zone 1 was mainly comprised of *Leptodiaptomus ashlandi* (29.7%), *L. sicilis* (15.5%), *Diacyclops thomasi* (10.1%) and copepod nauplii (9.8%) (Figure 12). Zone 2 biomass was dominated by many of the same groups with *L. ashlandi* remaining around 30% and *L. sicilis* increasing to 41.4%, but also *L. minutus* (13.1%). In Zone 3, zooplankton was mainly comprised of *L. sicilis* (38.8%), *L. ashlandi* (25.8%) and L. minutus (12.3%). In May 2019, zooplankton biomass in Zone 1 was composed of *D. thomasi* (22.9%), *L. ashlandi* (18.4%), *copepod nauplii* (9.0%) and *L. sicilis* (8.6%)(Figure 12). Zooplankton in Zone 2 was composed of *L. ashlandi* (28.6%), *L. sicilis* (17.1%), and *L. minutus* (11.2%). Offshore in Zone 4, biomass was comprised mainly of *L. ashlandi* (23.7%), *L. sicilis* (23.3%), *D. thomasi* (14.4%) and *L. minutus* (12.8%).

5.6 Zooplankton size composition relative to the thermal bar

The relative size composition of zooplankton biomass varied among zones along the Muskegon transect in April and May of 2015 and 2019 (Figure 13). In April 2015, size bins 1-2 biomass represented the largest proportion nearshore (Zone 1) declining in Zone 2 as proportion of bins 3-4 increased. Toward offshore (Zone 3), there were equal proportions of size bins 1-4, and further (Zone 4) bins 3-4 were dominant. In May 2015, size bins 1-3 zooplankton comprised the largest biomass proportion nearshore in Zone 1 but bins 3-4 became dominant in Zone 2 as relative biomass of the smaller zooplankton declined. Offshore (Zones 3 and 4), bins 3-4 represented the highest biomass.

In April 2019, relative biomass proportion of size bins 1-2 zooplankton decreased from nearshore (Zone 1) to offshore (Zone 3) as the proportion of bin sizes 3-4 increased. Farther offshore in Zone 4, bin sizes 3-4 were dominant. In May 2019, the proportion of bin sizes 1-2 was lower in nearshore zones than bins 3-4. Offshore in Zone 3, the proportions of most size bins decreased (except bin 3) relative to Zone 2. In Zone 4, the proportions of all bins decreased relative to Zone 3 except bin size 1.

5.7 Chlorophyll biomass, temperature, PAR and CDOM around the thermal bar

Environmental characteristics of zones relative to the thermal bar along the Muskegon transect varied among months and years. CHL biomass decreased with

distance to shore from Zones 1 to 4 (Figure 14). Zones 1 and 2 had higher chlorophyll biomass in 2015 than in 2019 in both April and May. In April 2015 and 2019, chlorophyll biomass was higher in areas inshore of the thermal bar than in areas offshore of the thermal bar. In May 2015, chlorophyll biomass in Zone 1 was higher than other zones, but in May 2019, chlorophyll biomass was highest in Zone 4.

Water temperature decreased steadily from Zone 1 to Zone 4 each year (Figure 15). In April, temperature nearshore was similar in 2015 and 2019 while in May, Zone 1 temperature reached 6.5℃ in 2015 but was lower in 2015. The average temperature in Zone 4 was higher in May than in April in both years.

There was no pattern of PAR among four zones. PAR varied among months. May 2019 had the highest PAR in Zone 1 and Zone 2 and April 2015 had the highest PAR in Zone 3 and Zone 4 (Figure 16).

CDOM decreased from Zone 1 to Zone 4 in both months and years, and was much higher in 2015 than in 2019 (Figure 17). In 2015, CDOM in April was much higher than May while in 2019 it was similar in April and May.

6 Discussion

6.1 Thermal bar temporal dynamics

The range in dates of thermal bar formation (March 14 - April 28) and disappearance (April 1 - May 29) found in this study is consistent with dates reported in a previous study for southern Lake Michigan by Fichot et al (2019), and support the hypothesis that years with warmer springs have an earlier thermal bar formation date than in colder springs. Thermal bar formation dates in my study also are consistent with those reported by Ullman et al (1998), but disappearance dates I found are earlier. While Fichot et al.'s (2019) study was conducted from 1995-2012, Ullman et al (1998) reported a later disappearance date (July) for earlier observations of the thermal bar made from 1985 to 1995. An earlier disappearance of thermal bars in this study can be explained by warmer weather as the monthly April to June air temperatures at Muskegon were on average 2℃ warmer than in 1985-1995 (https://www.wunderground.com/). It also is possible that the thermal bar along the Muskegon transect in this study was not observed by Ullman et al (1998), who reported that thermal bars occurred only in several sites along the southern Lake Michigan shoreline and covered less than 5% of the shoreline in June.

6.2 Thermal bar speed

Thermal bar speeds estimated in this study to range from 0 to 3.53 cm/s are within the range of other estimates for Lake Michigan but exceed reports for Lake Ontario. The lowest speed I estimated was slower than that reported by Fichot et al (2019) for

southern Lake Michigan, but it is possible that the coarse spatial resolution of AVHRR SST data used in this study, where a pixel represents 0.76 km, could not accurately capture such short thermal bar movements. Other estimates of thermal bar speed of 0.21 cm/s during 1988 near the Muskegon transect (Moll et al. 1993) and of 0.44 to 1.74 cm/s in southwestern Lake Michigan during 2007-2009 (Wang, 2013) are within the range in my study.

My estimates of thermal bar speed along the Muskegon transect exceeded the range of 0.3-0.95 cm/s in a study by Elliott (1970) using a model for Lake Ontario. A lower thermal bar speed can be expected for Lake Ontario because the bottom slope is much steeper than along the Muskegon transect in Lake Michigan. Furthermore, the model simulated the thermal bar under more stable water column conditions than in this study.

Results of GLMs on the influence of lake conditions on the thermal bar speed were partially consistent with previous studies and support the hypothesis that air temperature has a significant effect on speed. This finding is in agreement with studies by Bennett (1971), Rodgers (1987) and Moll et al (1993), and supports the idea that warming from solar insolation is a basic driver of thermal bar movement. My finding that thermal bar speed increased with distance to shore, where bottom slope increases, are consistent with those of Fichot et al (2019) and Wang (2013), but do not agree with earlier reports that speed is slower in offshore areas with steeper bottom slopes than in nearshore areas (MaIm and Jonsson,1993; Spain et al 1976).

GLM results did not support the hypothesis that runoff discharge has a significant effect on thermal bar speed. The lack of a significant effect of runoff discharge on thermal bar speed contrasts with previous findings by Moll et al (1993) that runoff discharge drives thermal bar speed in early spring. Spain et al (1976) claimed that a steep bottom slope would slow thermal bar speed by slowing the rate of entry of offshore water from the lake bottom. This was not the case for surface movement of the thermal bar in this study because movement was most impacted by air temperature. The faster speed offshore in this study may be caused by the tilting of the thermal bar and high variation in surface water temperatures. As the thermal bar moves farther offshore, a larger proportion of the heating sources comes from solar radiation, and as water temperature decreases with depth, the thermal bar at the surface moves faster than the thermal bar at the bottom. The vertical heating exchange was limited near the thermal bar due to tilting of thermal bar. As surface water temperatures are very sensitive to air temperature changes, high air temperature can lead to rapid increases in surface water temperature and increase speed of the thermal bar at surface when thermal bar is tilted offshore.

6.3 Zooplankton biomass distribution

GLMs results generally supported the hypothesis that zooplankton biomass is higher

inshore of the thermal bar compared to offshore of the thermal bar, and are consistent with seasonal distribution patterns reported by Agy (2001). Higher zooplankton biomass inshore from the thermal bar may result from retainment of CDOM, nutrients and chlorophyll at the thermal bar by convergent flows from inshore and offshore. The lone exception to this pattern of higher zooplankton biomass inshore of the thermal bar occurred in April 2019, after a large river runoff event in late March and early April had discharged CDOM and plankton into the nearshore zone. The zooplankton remained offshore of, but close to the thermal bar after it formed later in April 2019.

Temporal-spatial distributions of zooplankton biomass around the thermal bar in this study were similar to those reported in Lake Baikal by Tsydenov (2019). At the initial stage of thermal bar formation, zooplankton biomass was highest nearshore in both studies. When the thermal bar moved offshore in Lake Baikal, the highest zooplankton biomass remained nearshore similar to in this study in May 2015. At the initial stage of the thermal bar, in both studies zooplankton biomass was highest nearshore because of higher chlorophyll biomass and warmer water conditions nearshore than offshore. However, in May 2019, zooplankton biomass was highest in inshore areas close to the thermal bar mainly due to increased biomass of calanoid copepods close to the thermal bar. This could possibly be a consequence of an early spring runoff event, phytoplankton particle sizes, cooler water temperatures and convergent flows.

6.4 Zooplankton species and size composition around the thermal bar

Temporal changes in the relative biomass composition of large copepod species in nearshore areas may reflect differences in the species' reproductive cycles, and temperature and feeding preferences. For example, biomass of the relatively large copepod *Leptodiaptomus sicilis* in nearshore areas decreased significantly as temperature warmed from April to May, and was replaced by smaller copepods (copepod nauplii, Diaptomid copepodite stages (C1-C5), *L. minutus*) in 2015 and by *Diacyclops thomasi* in 2019, respectively. This result is consistent with findings by Pothoven and Fahnenstiel (2015) and Agy (2001) that copepods in offshore colder areas were larger than in nearshore areas, especially in summer. *L. sicilis* is usually found in cooler and deeper waters than other copepods (Balcer et al, 1984). As temperatures increased in May, *L. sicilis* decreased nearshore while a higher proportion of other copepods remained. *L. sicilis* breeds between January and May, and immature persist in large numbers throughout the winter (Balcer et al, 1984; Selgeby, 1975). *L. ashlandi* begins breeding in April (Torke 2001) and *Diacyclops thomasi* begins breeding in March (Troke, 1975). Therefore, the relative proportion of *L. ashlandi*, *L. minutus*, *D. thomasi* and immature copepods increased in May due to development and growth. *L. sicilis* prefers feeding on particles > 53µm that are abundant in phytoplankton blooms, *L. ashlandi* and *L. minutus* prefer smaller particles <10 µm, and <20 µm respectively (Bowers, 1980) while *D. thomasi* prefers particles

between 15-100 µm (LeBlanc et al, 1997). As the phytoplankton blooms in May, the proportion of microplankton (>20 µm) decreases significantly in southeast Lake Michigan (Carrick et al, 2015). These factors may have led to a decline in the relative proportion of *L. sicilis* in the zooplankton biomass nearshore and an increase near the thermal bar and at offshore areas in May.

The spatio-temporal distribution of zooplankton biomass composition based on net tow sampling data is consistent with the laser optical plankton counter (LOPC) analysis of zooplankton size bins. The higher proportion of copepod nauplii in Zone 1 than in other zones in 2015 and 2019 in April and May is consistent with the higher proportions of zooplankton size bin 1 and bin 2 in that zone in both years and months. Further, higher proportions of bin 3 and bin 4 sized zooplankton in Zone 2 compared to Zone 1 also is consistent with higher proportions of larger zooplankton (*L. sicilis*, *L. ashlandi, L. minutus*). In April 2019, there was a higher proportion of bin 1 and bin 2 sized zooplankton inshore of the thermal bar compared to 2015, which is consistent with the net tow data that showed higher proportions of copepod nauplii and Diaptomid copepodite stages C1-C5 in Zone 2. In May 2019, there was a lower proportion of bin 1 and bin 2 sized zooplankton inshore of the thermal bar compared to 2015, and lower relative proportions of copepod nauplii and Diaptomid copepodite stages C1-C5 observed in net tows.

6.5 Chlorophyll a biomass distribution

Chlorophyll a (CHL) biomass differences found between inshore and offshore of the thermal bar in April 2015, April 2019 and May 2015 support the hypothesis that CHL biomass was higher in zones inshore than offshore of the thermal bar. The higher biomass inshore was likely influenced by higher CDOM concentrations and water temperatures found there. However, in May 2019, biomass was higher in offshore areas compared to areas inshore of the thermal bar, and did not match the distribution of high CDOM and water temperatures. This apparent discrepancy in distribution of chlorophyll may have been caused by the period when data were collected. Analysis was conducted of all PSS data collected during daylight in order to report PAR conditions for zooplankton. However, in May 2019, CHL biomass collected by PSS during the previous night indicated biomass was highest inshore relative to offshore, but the next day had declined to a lower level than biomass offshore.

CHL biomass differences found between inshore and offshore from the thermal bar generally are consistent with dynamics reported by Moll et al (1993). In both studies, at the initial stage of the thermal bar, zones inshore from the thermal bar had twice the CHL biomass of offshore zones. In the study by Moll et al (1993), when the thermal bar was located at mid-depth areas on April 29 1988, CHL biomass in zones inshore of the thermal bar was less than 20% higher than the zones offshore from the thermal

bar. In this study when the thermal bar was located at offshore and mid-depth areas respectively in May 2015 and 2019, CHL biomass in zones inshore from the thermal bar was less than 50% higher than offshore zones.

Distribution of CHL biomass around the thermal bar appears to differ from an earlier study in southeast Lake Michigan conducted in April 1988 (Moll et al, 1993) and in Lake Baikal in June 2017 (Tsydenov, 2019). During the initial stage of thermal bar formation, the highest biomass of chlorophyll was observed in the nearshore areas of Lake Michigan and Lake Baikal in those studies. However, when the thermal bar was located at mid-depth or offshore areas, Tsydenov (2019) reported that chlorophyll biomass was highest in offshore areas close to the thermal bar, and Moll et al. (1993) reported that chlorophyll biomass at the thermal bar was 6.8% and 24.2% higher in mid-depth areas compared to nearshore and offshore areas. Tsydenov et al (2019) suggested that wind-driven currents were responsible for Lake Baikal chlorophyll biomass to be highest in offshore areas and near the thermal bar. Moll et al (1993) concluded that higher chlorophyll biomass at the thermal bar in mid-depth area compared to nearshore was explained by the similar water temperature and convergence flow towards thermal bar. In my study, the highest CHL biomass nearshore in April 2015, April 2019 and May 2015 can be explained by warmer water and highest CDOM nearshore compared to the mid-depth area and offshore. In May 2019, the higher CHL biomass offshore compared to nearshore may be explained by grazing effects of higher zooplankton biomass nearshore than offshore. Alternatively, this result could be an artifact of daylight quenching measures of chlorophyll in the fluorometer, as chlorophyll measures made the previous night on that survey indicated chlorophyll was higher nearshore than offshore.

6.6 Significance of thermal bars for biological processes

This study contributes to a deeper understanding of the thermal bar dynamics and its impact on zooplankton biomass, species composition and distribution. Use of the fluorometer and laser optical plankton counter for PSS data in this study helped to more accurately define thermal bar characteristics and biomass distributions of zooplankton relative to temperature, chlorophyll a, light and CDOM. The results show thermal bars can influence the zooplankton biomass distribution between inshore and offshore areas through retention of warmer water, chlorophyll and nutrients. Movement of the thermal bar from inshore to offshore led to the spread of plankton, warm water and organic material offshore. The CHL biomass difference between nearshore and offshore areas decreases as the thermal bar moves offshore, and also decreases the zooplankton biomass differences between nearshore and offshore. Analysis of zooplankton biomass composition suggested variation in species preference for aquatic environments nearshore and offshore of thermal bars. Further work with more targeted net-tow sampling within and among thermal bar zones will improve knowledge of how the lower food web, and particular zooplankton life stages (adults, nauplii, copepodites) will respond to variable warming conditions and inputs of organic matter.

Table 1. Data types analyzed and their relevance to this study of the spring thermal bar. Data were obtained from websites available from NOAA GLERL and USGS and from long-term research programs conducted by NOAA GLERL staff.

Project	Data type	Purpose
NOAA CoastWatch	AVHRR Sea Surface Temperature data	Identify thermal bar location
USGS: National Water Information System	Runoff discharge Runoff temperature	Explain thermal bar distance to shore and speed
NOAA GLERL: Real-Time Meteorological Observation Network	Air temperature	Explain thermal bar distance to shore and speed
NOAA GLERL : Plankton Survey System (PSS)	i) Net tow zooplankton data ii) 5 bin sized zooplankton biomass iii) Water Temperature; Chlorophyll a; Photosynthetically active radiation (PAR); Colored dissolved organic matter (CDOM)	Identify zooplankton biomass distribution and composition
NOAA GLERL: Long term research program (LTR)	Net tow zooplankton data Nutrients Chlorophyll a (CHL)	Identify zooplankton composition

Table 2. Data sources, sites and dates sampled by net tows in 2015 and 2019 for the analysis of zooplankton species distribution around the spring thermal bar along the Muskegon transect.

Year	Date	Station	Mesh net size	Sources
2015	March 24	M15; M45; M110	153 µm	LTR
2015	April 6	M15; M45; M110	153 µm	LTR
2015	April 14	M15; M45; M110	153 µm	LTR
2015	May 11	M15; M45; M110	153 µm	LTR
2015	June 1	M15; M45; M110	153 µm	LTR
2015	June 15	M15; M45; M110	153 µm	LTR
2015	April 28	M15; M110	153 µm	PSS
2015	May 20	M15; M110	153 µm	PSS
2019	April 29-May 2	M10; M15; M30	64 µm	PSS
2019	May 14-16	M15; M35; M110	64 µm	PSS

Table 3. Size range of equivalent spherical diameters (ESD) of optical plankton counter (OPC) bins and zooplankton taxa likely to fall in these bins (from Liebig and Vanderploeg 2008).

OPC bins	ESD Range	Zooplankton taxa
Bin 1	0.091-0.255 mm	nauplii, Bosmina longirostris, Diaptomid copepodite stages C1-C5, Veligers
Bin 2	0.256-0.495 mm	nauplii, Bosmina longirostris, Diaptomid copepodite stages C1-C5, small Leptodiaptomus ashlandi, small L. minutus, small L. sicilis, dreissena veligers, Diacyclops thomasi
Bin 3	0.496-0.750 mm	Diaptomid copepodite C1-C5, L. ashlandi, L. minutus. L. sicilis, D. thomasi
Bin 4	0.751-1.5 mm	L. sicilis, L. ashlandi, L. minutus, D. thomasi, Limnocalanus macrurus
Bin 5	1.501-4.005 mm	Limnocalanus macrurus

Table 4. Dates on which spring thermal bars were first and last observed, and thermal bar duration along the Muskegon transect in southeastern Lake Michigan from 2010 to 2019.

Year	Thermal bar first observed	Thermal bar last observed	Duration (days)
2010	April 12	April 26	15
2011	April 25	May 8	14
2012	March 14	April 1	19
2013	April 20	May 11	22
2014	May 17	May 29	13
2015	April 29	May 20	32
2016	April 22	April 28	7
2017	April 8	April 14	7
2018	April 26	May 5	10
2019	April 20	May 14	25

Table 5. Results of three General Linear Models (GLMs) to analyze variation in thermal bar distance to shore as a function of runoff temperature, air temperature, and average air temperature 7 days prior to thermal bar identification. Sample size = 41. The * indicates slopes were significant at the 90% level.

Model	Slope	t value	P of t Value
Runoff temperature	1.040	4.119	0.0002*
Average air temperature 7 days prior to thermal bar identification	1.244	5.099	9.17e-06 *
Air temperature	0.159	0.688	0.495

Table 6. Outputs of a GLM of the thermal bar speed as a function of average air temperature and average Muskegon River discharge, and a GLM of the thermal bar speed as a function of distance to shore. The * indicates slopes were significant at the 90% level.

Model	Variable	Slope	t value	P of t Value
Model 1	Average air temperature 10 days prior to the end of the movement	0.2767	2.146	0.055 *
	Runoff discharge	0.0004	1.610	0.136
Model 2	Distance to shore	0.1137	2.092	0.057 *

Table 7. Mean zooplankton biomass in wet weight (µg/l) in April and May of 2015 and 2019. Zone 1 was inshore and > 405 m from the thermal bar; Zone 2 was inshore and within 405 m of the thermal bar; Zone 3 was offshore and within 405 m of the thermal bar; Zone 4 was offshore and > 405 m from the thermal bar.

Year	Month	Zone 1	Zone 2	Zone 3	Zone 4
2015	April	1741 ± 57	1720 ± 74	748 ± 31	399 ± 3
	May	1624 ± 14	500 ± 12	210 ± 5	309 ± 3
2019	April	560 ± 13	562 ± 11	590 ± 16	373 ± 2
	May	379 ± 4	492 ± 12	344 ± 10	301 ± 3

Table 8. Zones relative to the thermal bar and corresponding sampling stations along the Muskegon transect for zooplankton data used in this study. Zone 1 = inshore and > 405 m from the thermal bar; Zone 2 =inshore and within 405 m of the thermal bar; Zone 3 = offshore and within 405 m of the thermal bar; Zone 4 = offshore and > 405 m from the thermal bar. 'n.d.' indicates no data collected at that zone.

Year	Date	Zone 1	Zone 2	Zone 3	Zone 4
2015	April 28	n.d.	M15	n.d.	M110
2015	May 20	M15	n.d.	n.d.	M110
2019	April 29-May 2	M10	M15	M30	n.d.
2019	May 14-16	M15	M35	n.d.	M110

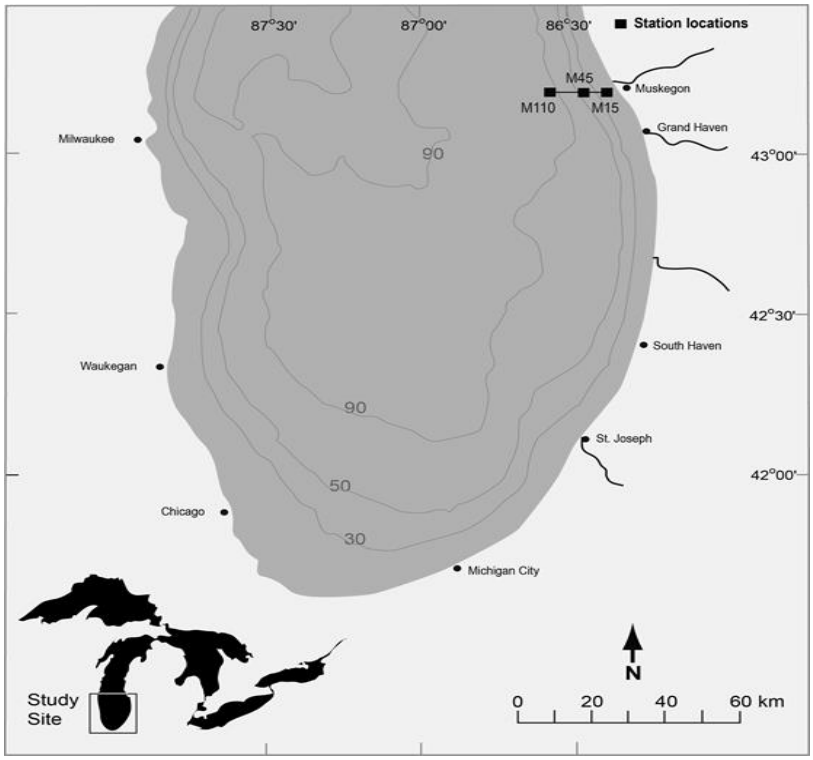

Figure 1. Bathymetric map of southern Lake Michigan indicating the location of stations of the long-term ecological research conducted by the NOAA Great Lakes Environmental Research Laboratory along the Muskegon transect at 15m, 45m and 110m in depth. Credit: Nicole Rice.

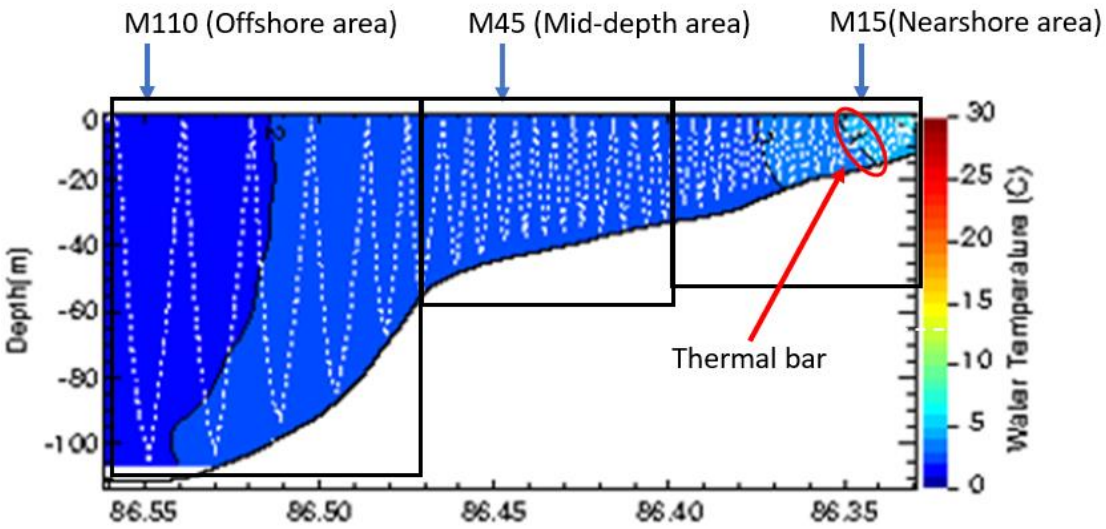

Figure 2. Sinusoidal path of the Plankton Survey System (PSS) towed during a cruise along a transect off Muskegon, MI on April 28, 2015. The white dotted line represents the path of the PSS shown on the water temperature-depth profile panel. Source: https://www.glerl.noaa.gov/res/PSS/2015/2015.04.2/

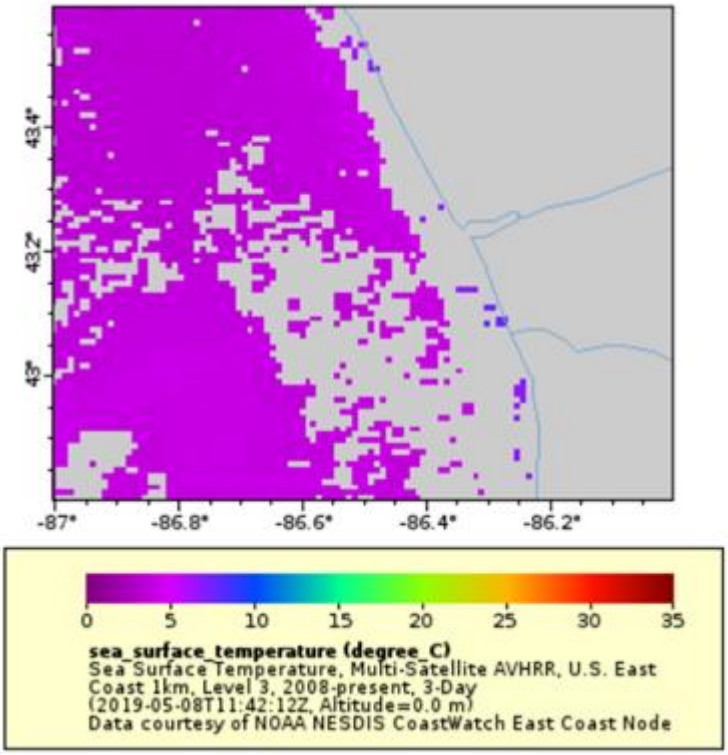

Figure 3. Example of a map of sea surface temperature from data collected at southeast Lake Michigan on May 8, 2019. Source: https://coastwatch.noaa.gov/erddap/griddap/noaacwecnAVHRRmultisatsstEastCoast3Day.graph

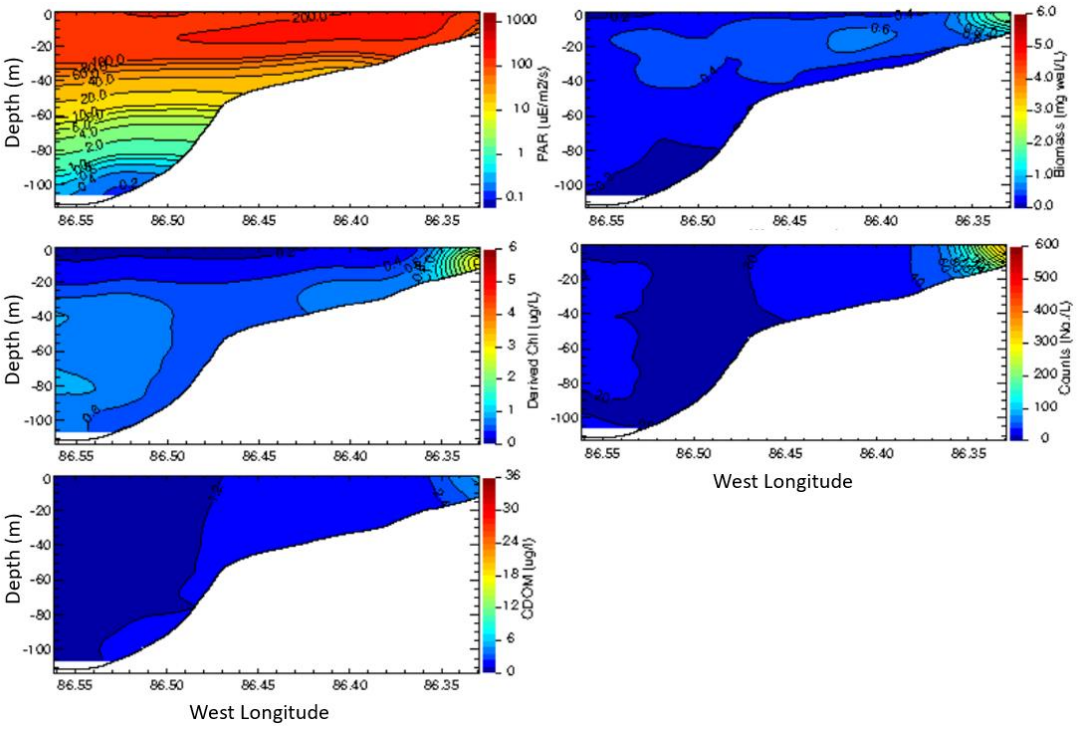

Figure 4. Example of photosynthetically active radiation (PAR), zooplankton biomass, CHL concentration data, zooplankton density and colored dissolved organic matter (CDOM) data collected by the Plankton Survey System along a transect off Muskegon, MI. Source: https://www.glerl.noaa.gov/res/PSS/2015/2015.04.2/

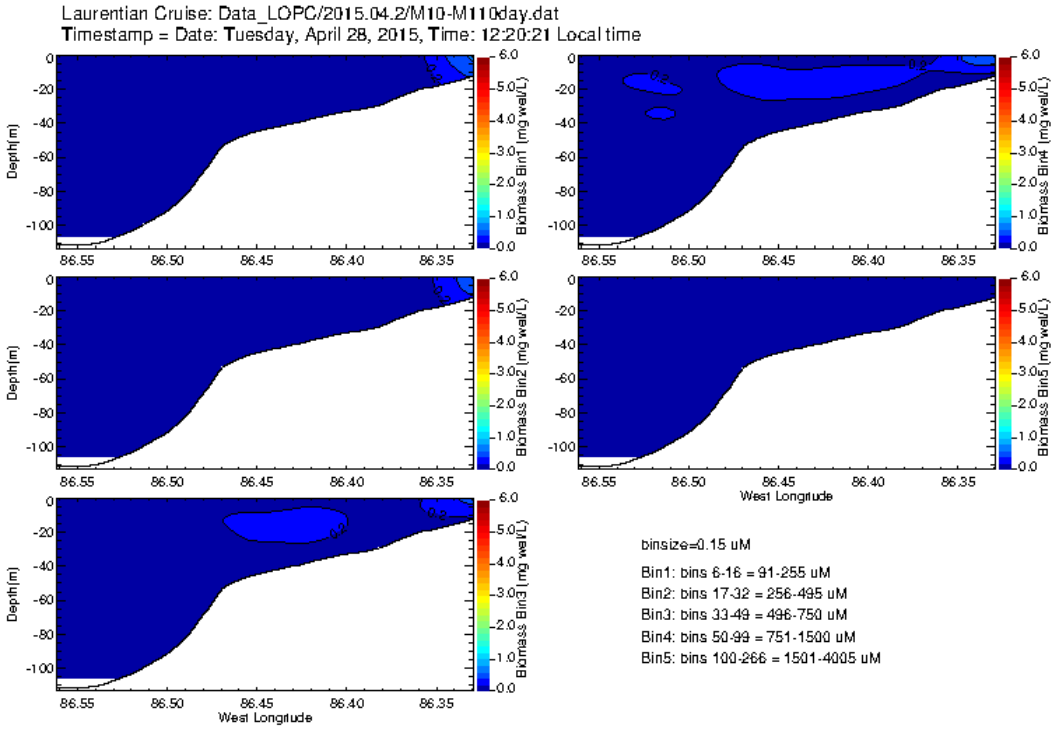

Figure 5. Example of zooplankton biomass data by five size categories (Bins 1 to 5) collected off Muskegon, MI. Source: https://www.glerl.noaa.gov/res/PSS/2015/2015.04.2/

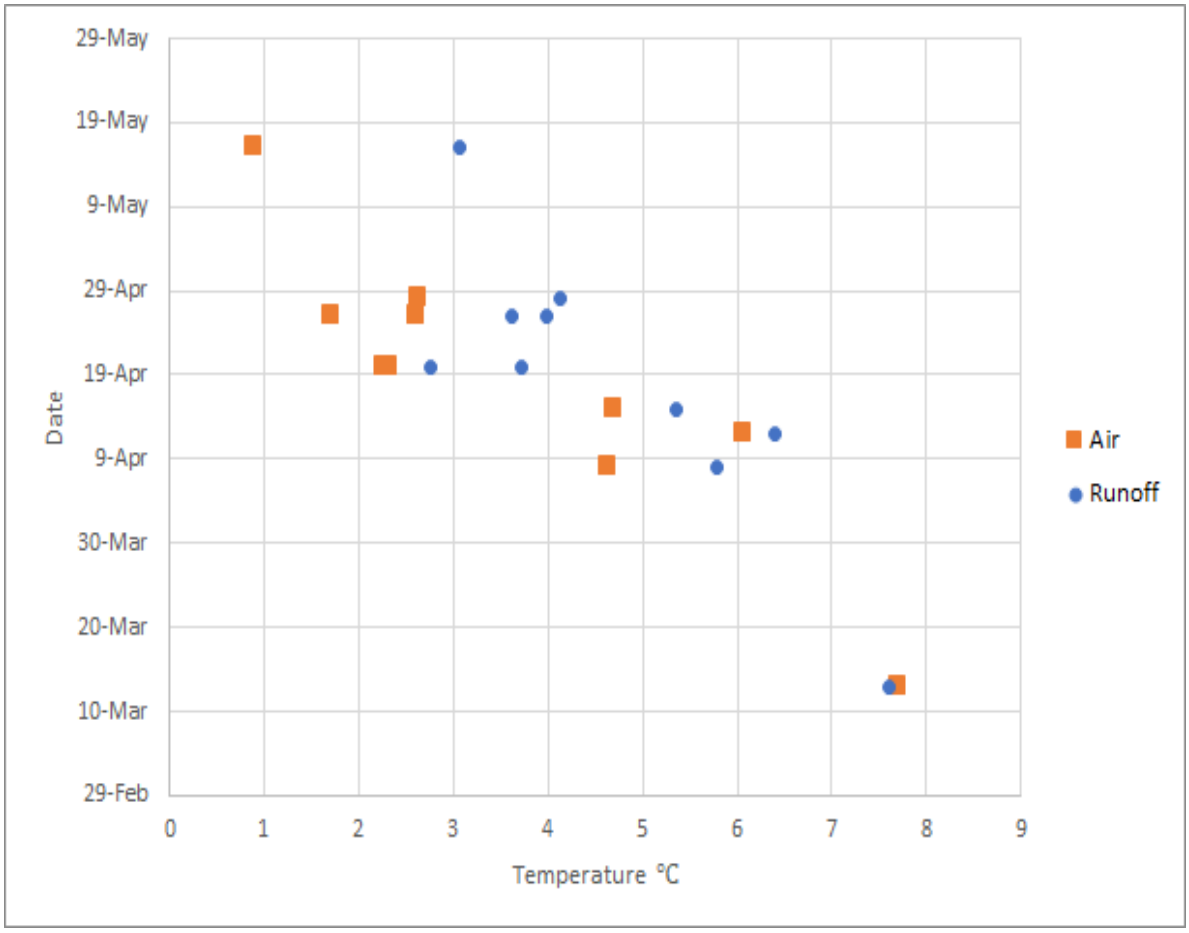

Figure 6. Thermal bar formation date in spring with average runoff and air temperature in nearshore southeast Lake Michigan, from 2010 to 2019.

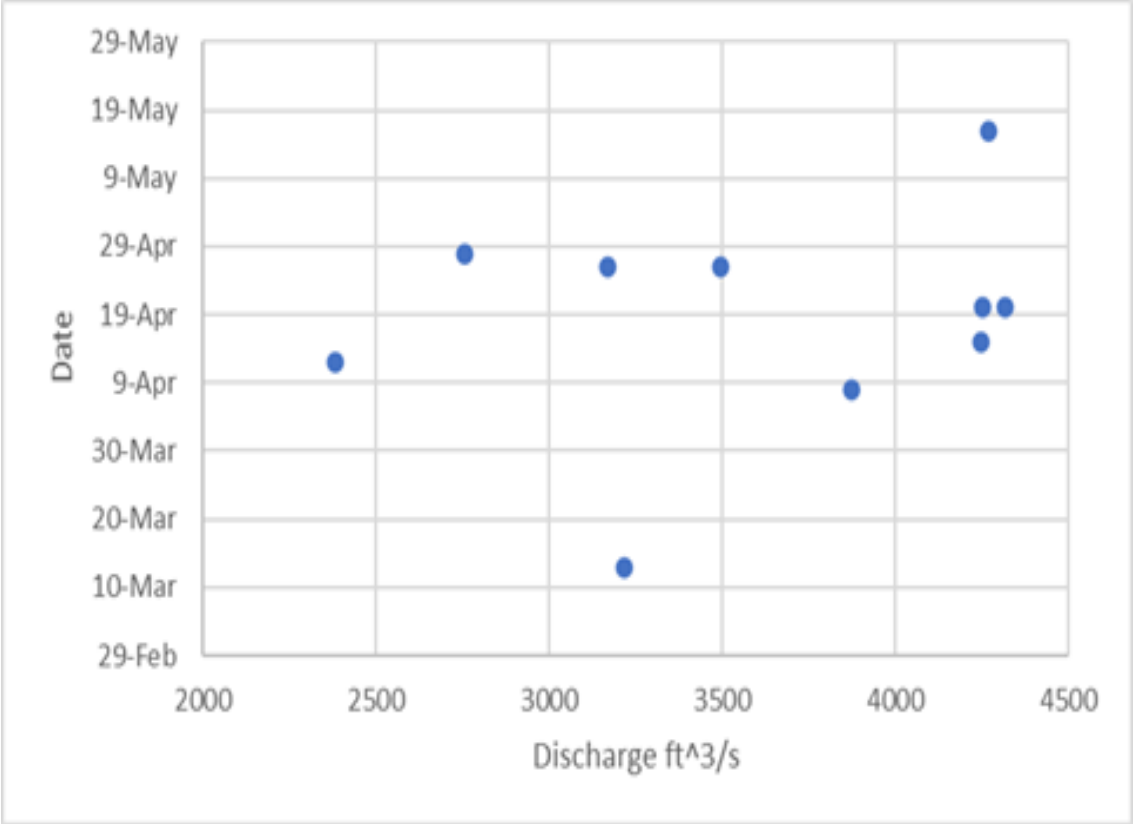

Figure 7. Thermal bar formation date in spring with average runoff discharge in the Muskegon River, MI from 2010 to 2019.

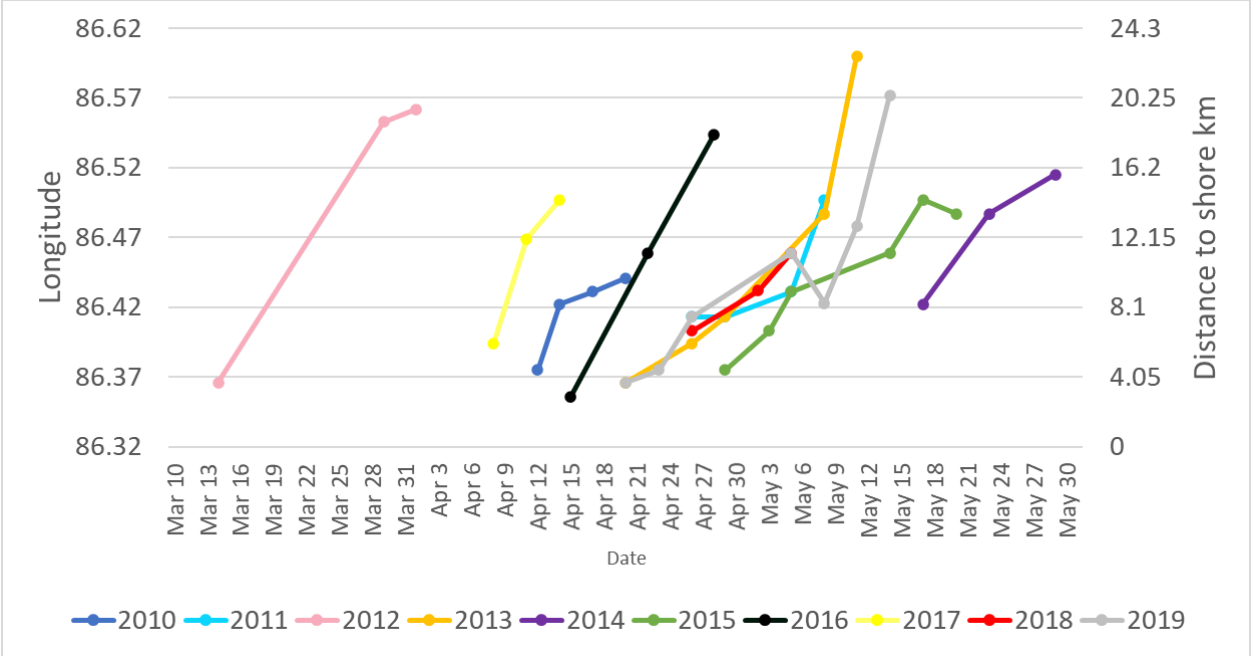

Figure 8. Location, start and end date of the spring thermal bars along the transect near Muskegon, MI from 2010 to 2019.

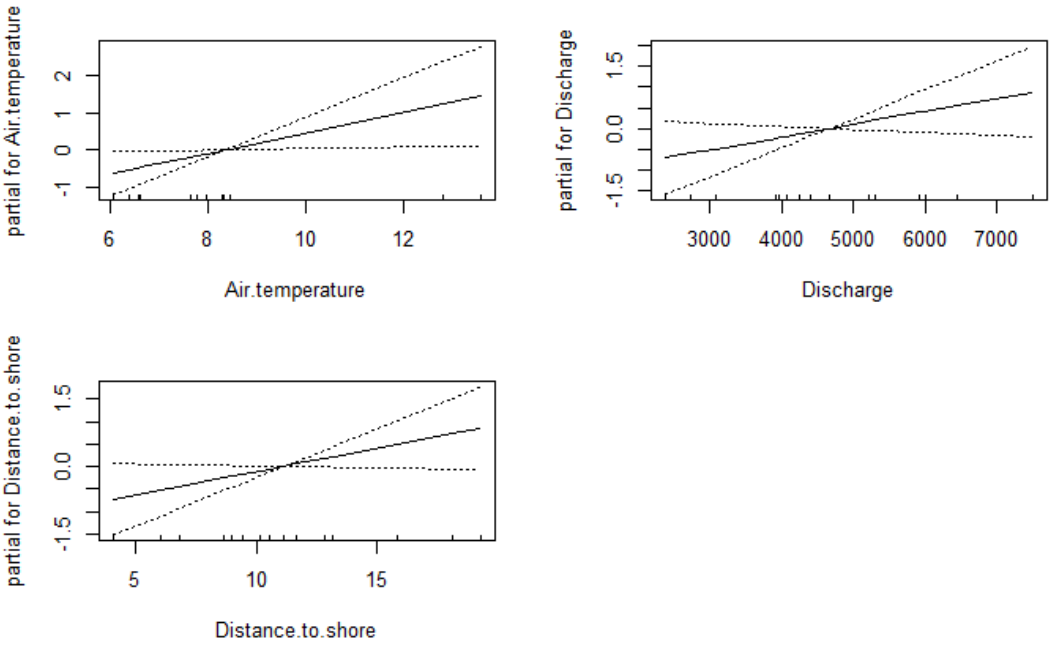

Figure 9. Outputs of (top) GLM for thermal bar speed as a function of air temperature and Muskegon River discharge; and (bottom) GLM for thermal bar speed as a function of distance to shore. The hash marks on the x-axis represent the number of observations. The y-axis represents the partial effect of each variable. The dotted lines indicate 95% confidence intervals.

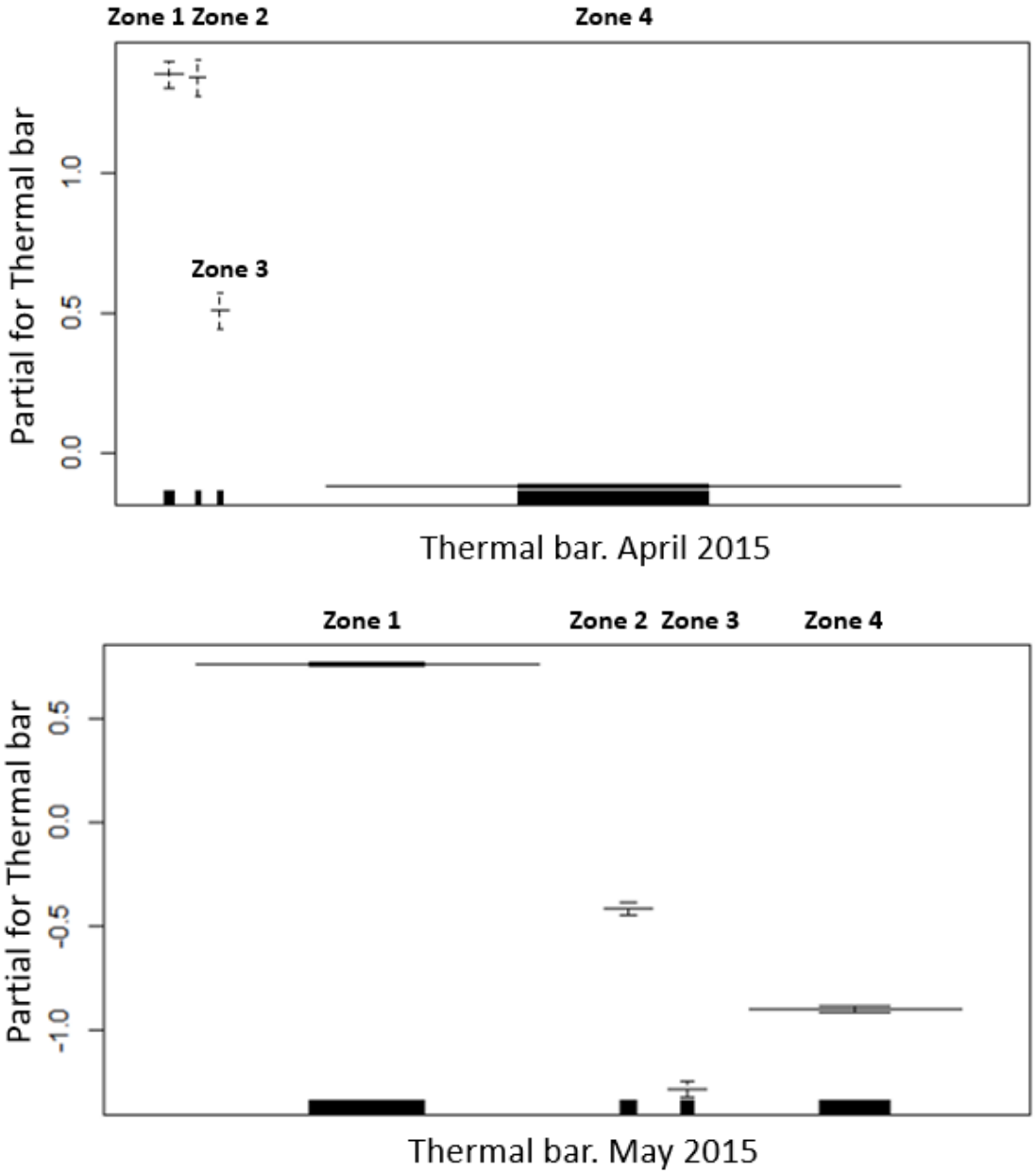

Figure 10. Results of GLMs for zooplankton biomass as a function of zones relative to the thermal bar location along the transect off Muskegon by month (April and May) in 2015. Zone 1 is inshore and > 405 m from the thermal bar; Zone 2 is inshore and within 405 m of the thermal bar; Zone 3 is offshore and within 405 m of the thermal bar; and Zone 4 is offshore and > 405 m from the thermal bar. Brackets represent two standard error bars. Zones with more data points have wider solid bars. The y-axis represents the partial effect of each zone.

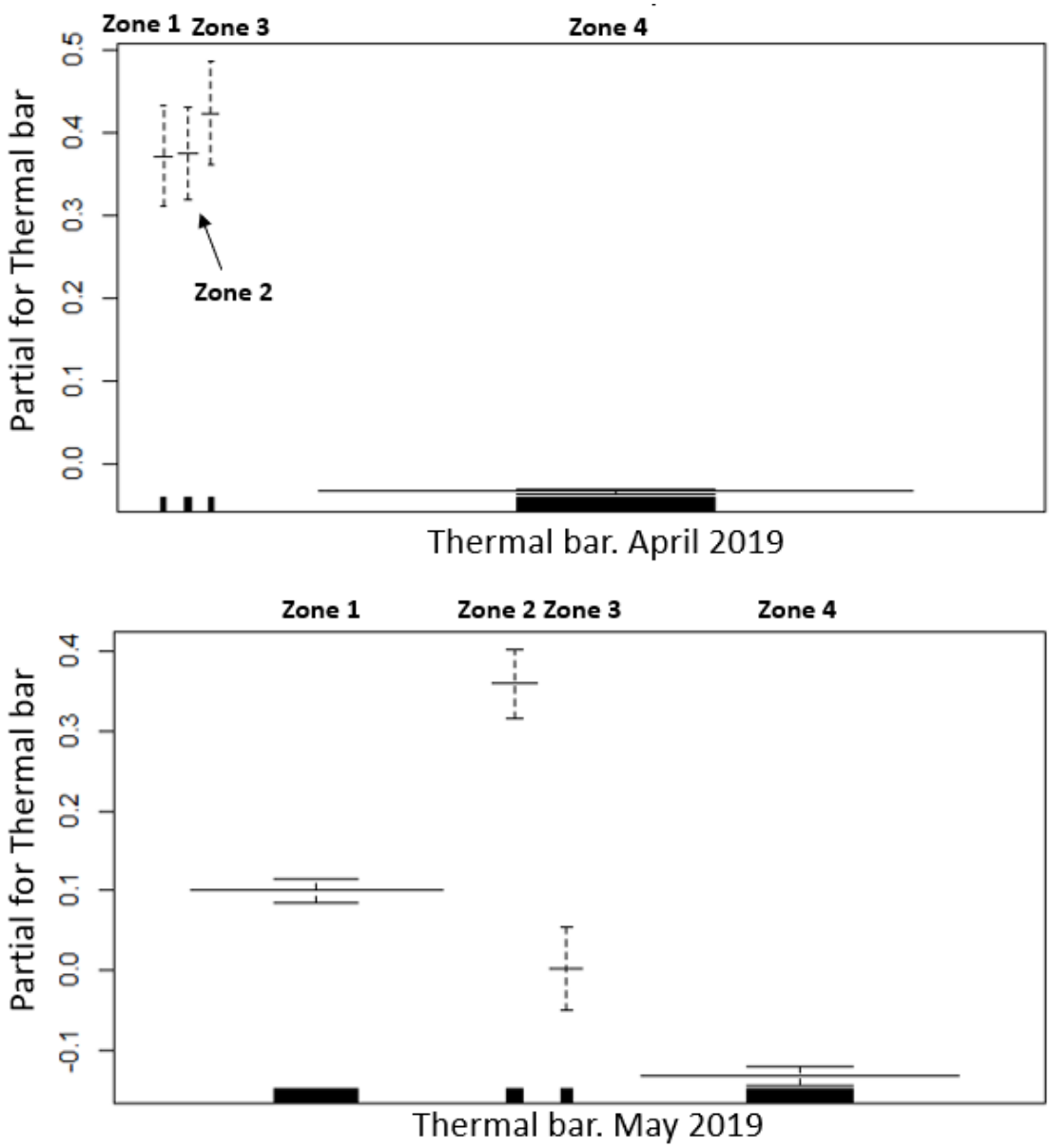

Figure 11. Results of GLMs for zooplankton biomass as a function of zones relative to the thermal bar location along the transect off Muskegon by month (April and May) in 2019. Zone 1 is inshore and > 405 m from the thermal bar; Zone 2 is inshore and within 405 m of the thermal bar; Zone 3 is offshore and within 405 m of the thermal bar; and Zone 4 is offshore and > 405 m from the thermal bar. Brackets represent two standard error bars. Zones with more data points have wider solid bars. The y-axis represents the partial effect of each zone.

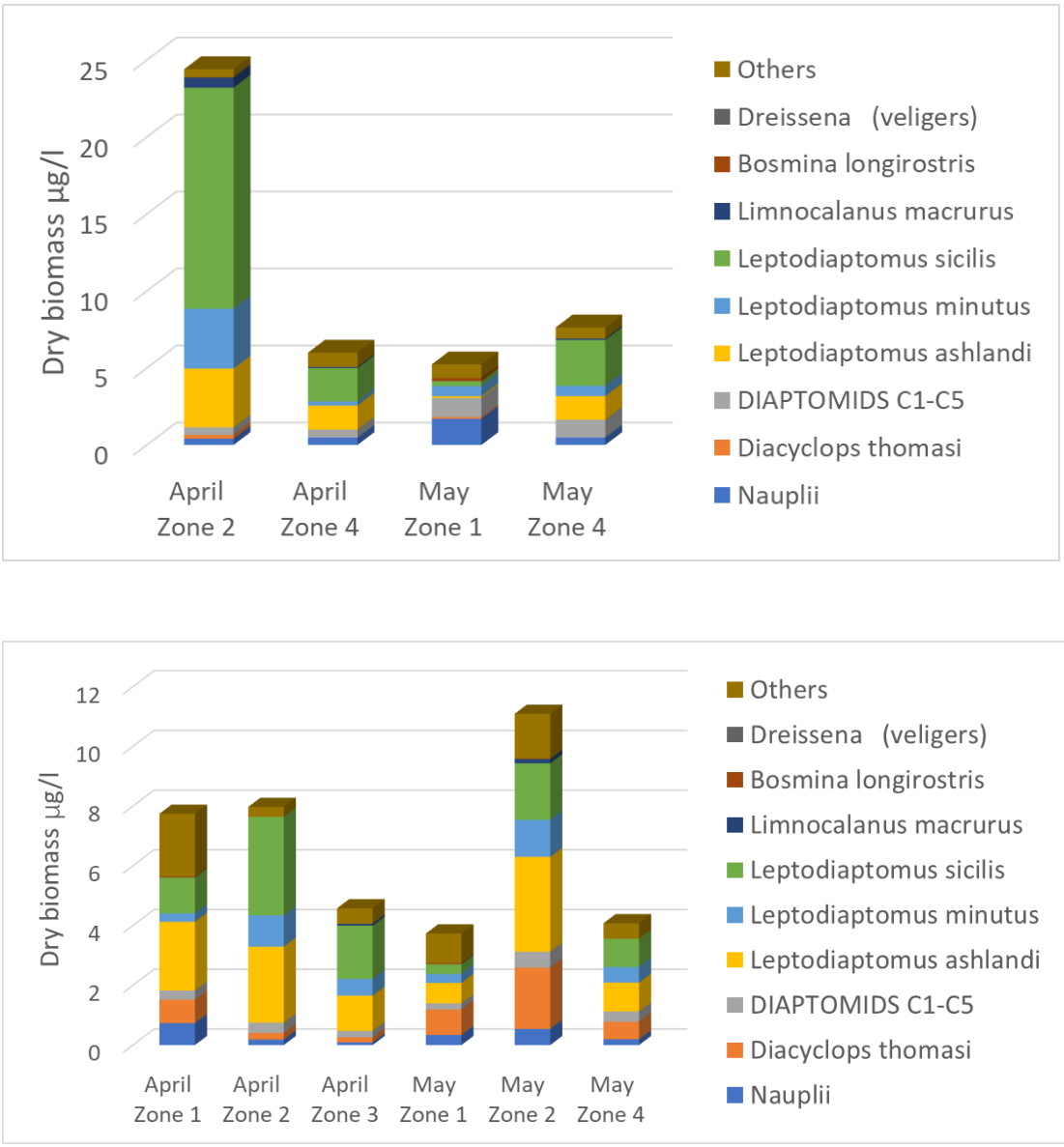

Figure 12. Species composition of zooplankton biomass (dry, µg/l) at zones relative to the thermal bar location along the transect off Muskegon in April and May in 2015 (top) and 2019 (bottom).

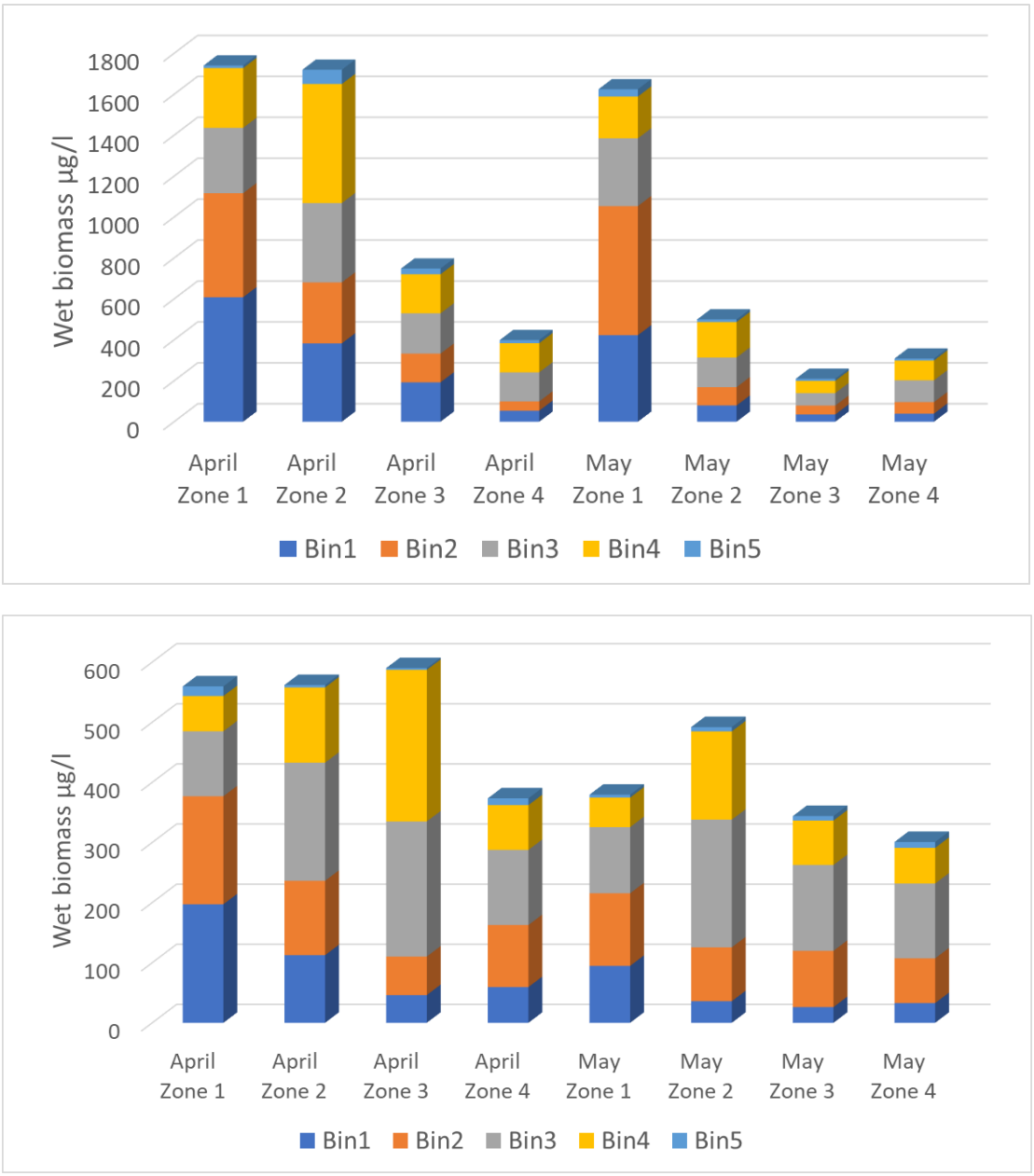

Figure 13. Zooplankton biomass (wet, µg/l) by spherical diameter size bins in four zones relative to the spring thermal bar along the Muskegon transect on April 28 and May 20 in 2015 (top), April 30 and May 14 2019 (bottom).

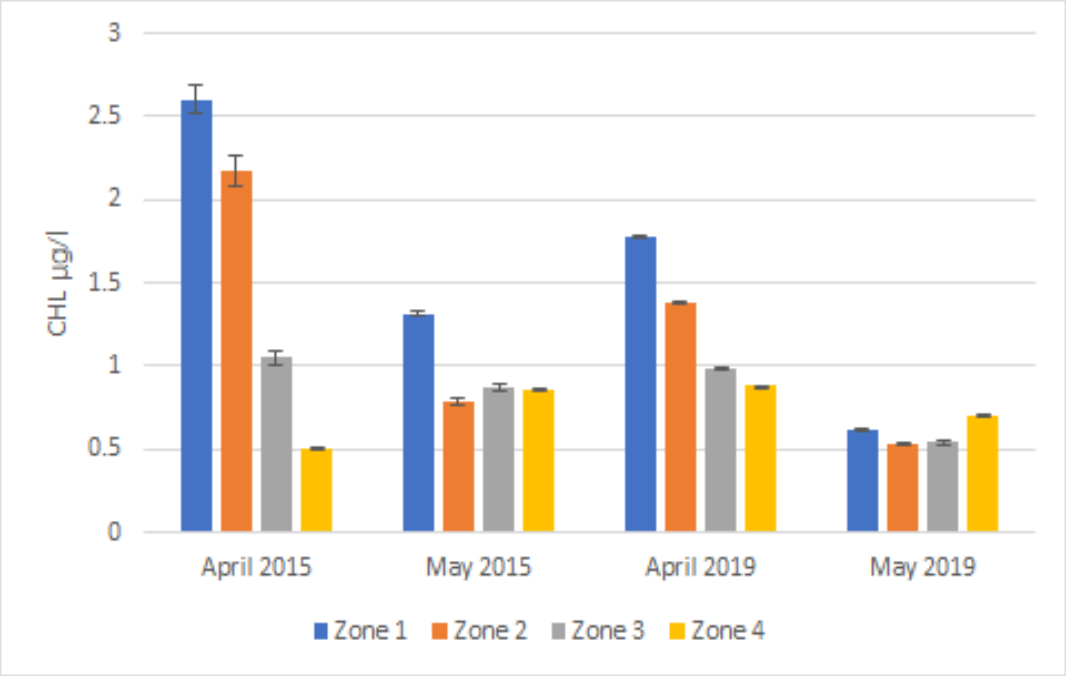

Figure 14. Chlorophyll a (CHL) biomass (µg/l) in four zones relative to the spring thermal bar along the Muskegon transect on April 28 2015, May 20 2015, April 30 2019 and May 14 2019.

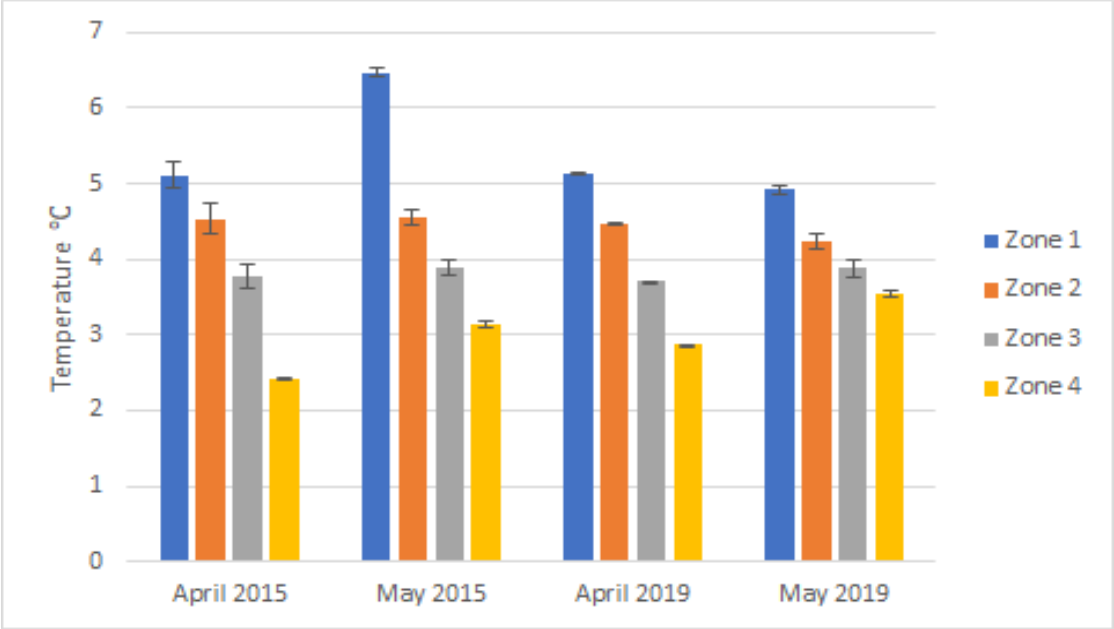

Figure 15. Water temperature (℃) in four zones around the spring thermal bar along the Muskegon transect on April 28 2015, May 20 2015, April 30 2019 and May 14 2019.

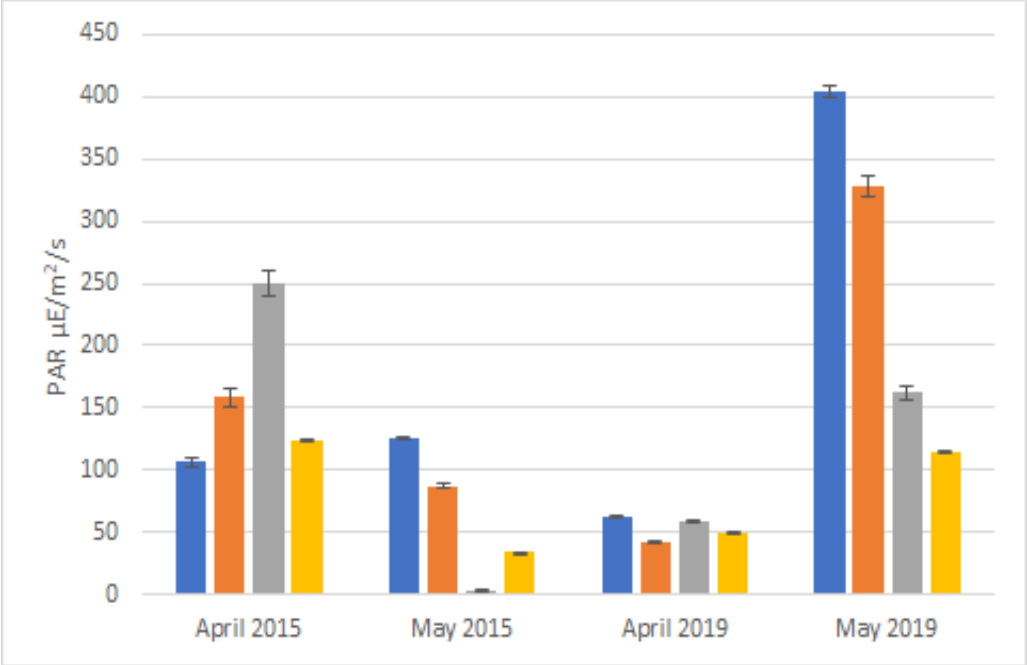

Figure 16. Photosynthetically active radiation (PAR) in four zones around the spring thermal bar along the Muskegon transect on April 28 2015, May 20 2015, April 30 2019 and May 14 2019.

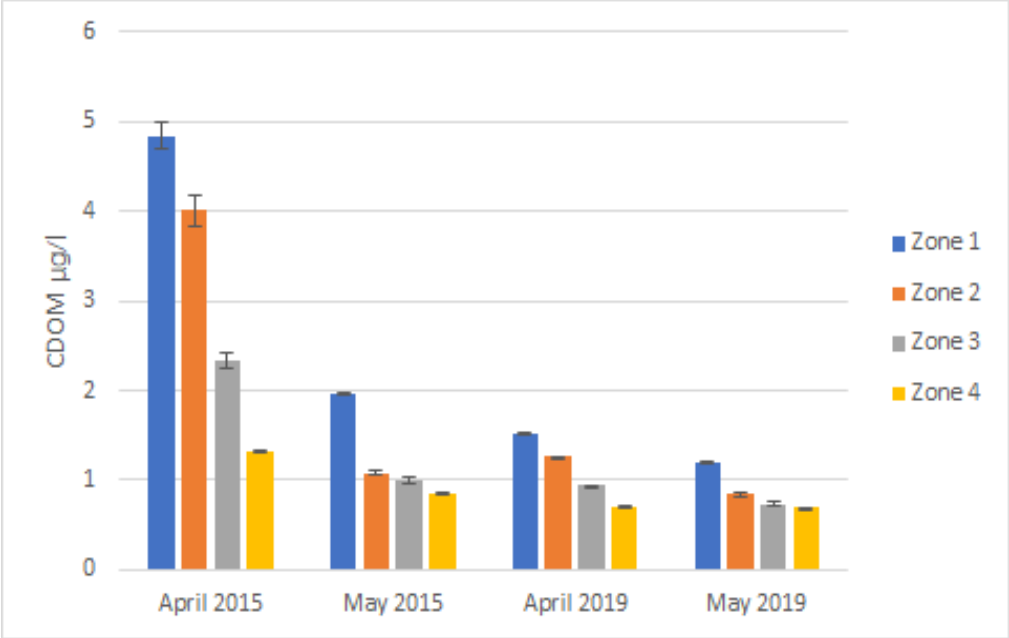

Figure 17. Colored dissolved organic matter (CDOM) in four zones around the spring thermal bar along the Muskegon transect on April 28 2015, May 20 2015, April 30 2019 and May 14 2019.

7 References

Agy, M. A. (2001), Changes in the nearshore and offshore zooplankton communities of southeastern Lake Michigan, M.S. thesis, Univ. of Mich., Ann Arbor

Auer, M. and Gatzke, T. (2004). The Spring Runoff Event, Thermal Bar Formation, and Cross Margin Transport in Lake Superior. J. Great Lakes Res. 30 (Supplement 1):64–81 Internat. Assoc. Great Lakes Res.

Balcer, M. D., Korda, N. L. and Dodson, S. I. (1984). Zooplankton of the Great Lakes—A Guide to the Identification and Ecology of Common Crustacean Species. University of Wisconsin Press, Madison.

Bennett, J. R. (1971). Thermally driven lake currents during spring and fall transition periods. In Proc. 14th Conf. Great Lakes Res., Internat. Assoc. Great Lakes Res., pp. 535-544.

Blokhina, N. S. (2015). The influence of wind on the development of a thermal bar and currents in reservoirs of different depths during ice cover melting. Mosc. Univ. Phys. Bull. 70 (4), 319–325. https://doi.org/10.3103/S0027134915040050

Bowers, J. A., Rossmann, R., Barres, J. and Chang, W. Y. B. (1986). Phytoplankton populations of southeast Lake Michigan 1974-1982, p. 141-168. In R. Rossmann (ed.), Impact of the Donald C. Cook Nuclear Plant. University of Michigan, Great Lakes Research Division, Publication number 22. Ann Arbor, Michigan.

Brandt, S. B. (1980). Spatial segregation of adult and young- of-the-year alewives across a thermocline in Lake Michigan. Transactions of the American Fisheries Society. 109:469-478.

Brandt, S. B. (1993). The effect of thermal fronts on fish growth - a bioenergetics evaluation of food and temperature. Estuaries 16: 142-159.

Brandt, S. B. and Wadley. V. A. (1981). Thermal fronts as ecotones and zoogeographic barriers in marine and fresh- water systems. Proceedings of the Ecological Society of Australia 11:13-26.

Brooks, J. L. (1959). Cladocera. In: Edmondson, W.T. (Ed.), Freshwater Biology. John Wiley and Sons, New York, pp. 587–656.

Bukreev, V. I. and Gavrilov, N. V. (2010). Instability of the thermal bar formed in a gravity current. Doklady Earth Sciences 430: 151-154.

Carrick, H., Butts, E., Daniels, D., Fehringer, M., Frazier, C., Fahnenstiel, G., Pothoven, S. and Vanderploeg, H. (2015). Variation in the abundance of pico, nano, and microplankton in Lake Michigan: Historic and basin-wide comparisons. Journal of Great Lakes Research, 41, 66-74. http://doi.org/10.1016/j.jglr.2015.09.009 .

Cayula, J. and Cornillon, P. (1992). Edge Detection Algorithm for SST Images, Journal of Atmospheric and Oceanic Technology, 9(1), 67-80.

Culver, D. A., Boucherle, M. M., Bean, D. J., and Fletcher, J. W. (1985). Biomass of freshwater crustacean zooplankton from length-weight regressions. Can. J. Fish. Aquat. Sci. 42: 1380-1390.

Dettmers, J. M., Raffenberg, M. J. and Weis, A. K. (2003). Exploring zooplankton changes in southern Lake Michigan: implications for yellow perch recruitment J. Great Lakes Res., 29, pp. 355-364.

Elliott, G. H. (1970). A Laboratory and Mathematical Study of the 'Thermal Bar'. Ph.D. Thesis, Inst. of Oceanogr., Univ. of British Columbia, Vancouver, B.C., Canada.

Evans, M. S. (1990). Large-lake responses to declines in the abundance of a major fish planktivore: the Lake Michigan example. Can. J. Fish. Aquat. Sci. 47, 1738–1754.

Fahnenstiel, G.L., Pothoven, S., Vanderploeg, H., Klarer, D., Nalepa, T. and Scavia, D. (2010). Recent changes in primary production and phytoplankton in the offshore region of southeastern Lake Michigan. J. Great Lakes Res. 36 (Suppl. 3), 20–29.

Fahnenstiel, G.L., Sayers, M.J., Shuchman, R.A., Yousef, F. and Pothoven, S.A. (2016). Lake-wide phytoplankton production and abundance in the Upper Great Lakes: 2010–2013. J. Great Lakes Res., 42 (2016), pp. 619-629

Holland, P. R. and Kay, A. (2003). A review of the physics and ecological implications of the thermal bar circulation. Limnologica. 33 (3), 153–162. https://doi.org/10.1016/S0075-9511(03)80011-7.

Huang, J. C. K. (1972). The thermal bar. Geophysical Fluid Dynamics 3:1–25.

Blanton, J.O. (1986). Coastal frontal zones as barriers to offshore fluxes of contaminants. Rapp. P.-V. Cons. Int. Explor. Mer. 186:18–30.

Jasper, S., Carmack, E. G., Dally, R. J., Gray, C. B. J., Pharo, C. H. and Wiegand, R. C. (1983). Primary productivity in a large, temperate lake with river interflow: Kootenay Lake, British Columbia. Can. J. Fish. Aquat. Sci. 40: 319-327.

Lathrop, R. G. Jr., Vande Castle, J. R. and Lillesand, T. M. (1990). Monitoring river plume transport and mesoscale circulation in Green Bay, Lake Michigan, through satellite remote sensing. J. Great Lakes Res. 16: 471–484.

LeBlanc, J. S., Taylor, W.D. and Johannsson, O.E. (1997). The feeding ecology of the cyclopoid copepod Diacyclops thomasi in Lake Ontario. J. Great Lakes Res. 23:369-381.

Liebig, J. R. and Vanderploeg, H. A. (2008). Selecting optical plankton counter size bins to optimize zooplankton information in Great Lakes studies. NOAA Technical Memorandum GLERL-143. ftp://ftp.glerl.noaa.gov/publications/tech_reports/glerl-143/tm- 143.pdf.

Madenjian, C. P., Fahnenstiel, G. L., Johengen, T. H., Nalepa, T. F., Vanderploeg, H. A., Fleischer, G. W., Schneeberger, P. J., Benjamin, D. M., Smith, E. B., Bence, J. R., Rutherford, E. S., Lavis, D. S., Robertson, D. M., Jude, D. J. and Ebener, M. P. (2002). Dynamics of the Lake Michigan food web, 1970-2000. Can. J. Fish. Aquat. Sci. 60:736-753.

Malley, D. F., Lawrence, S. G., MacIver, M. A., and Findlay, W. J. (1989). Range of variation in estimates of dry weight for planktonic crustacea and rotifera from temperate North American lakes. Can. Tech. Rep. Fish. Aquat. Sci. No. 1666, Dept. of Fisheries and Oceans, Winnipeg, Manitoba.

Malm, J., and Jonsson, L. (1993). A study of the thermal bar in Lake Ladoga using water surface temperature data from satellite images. Remote Sens. Environ. 44:35-46.

McCullagh, P., and Nelder, J.A. (1989). Generalized Linear Models. Second. London: Chapman; Hall/CRC. https://www.crcpress.com/p/book/9780412317606.

Miller, T.J., Crowder, L. B., Rice, J. A. and Marschall, E. A. (1988). Larval size and recruitment mechanisms in fishes: toward a conceptual framework. Canadian Journal of Fisheries and Aquatic Sciences 45(9):1657-1670

Miller, T.J., Crowder, L. B., Rice, J. A. and Binkowski, F. P. (1992). Body Size and the Ontogeny of the Functional Response in Fishes. Canadian Journal of Fisheries and Aquatic Sciences 49(4):805-812

Moll, R.A., Bratkovich, A., Chang, W. Y. B. and Pu, P. (1993). Physical, chemical, and biological conditions associated with the early stages of the Lake Michigan vernal thermal front. Estuaries 16, 92–103 (1993). https://doi.org/10.2307/1352767

Mortimer, C. H. (1988) . Discoveries and testable hypotheses arising from coastal zone color scanner imagery of southern Lake Michigan. Limnol. Oceanogr. 33: 203-226.

Nalepa, T. F., Fanslow, D. L., and Lang, G. A. (2000). Trends in benthic macroinvertebrate populations in southern Lake Michigan over the past several decades. Internationale Vereinigung fár Theoretische und Angewandte Limnologie Verhandlungen, 27: 2540–2545.

Owen, R. W. (1981). Fronts and eddies in the sea: Mechanisms, interactions and biological effects, p. 197-233. In A. R. Long-hurst (ed.), Analyses of Marine Ecosystems. Academic Press, London.

Pothoven, S. A. and Fahnenstiel, G. L. (2015). Spatial and temporal trends in zooplankton assemblages along a nearshore to offshore transect in southeastern Lake Michigan from 2007 to 2012, Journal of Great Lakes Research, Volume 41, Supplement 3, Pages 95-103, ISSN 0380-1330, https://doi.org/10.1016/j.jglr.2014.09.015.

R Core Team (2013). R: A language and environment for statistical computing. R Foundation for Statistical Computing, Vienna, Austria. URL http://www.R-project.org/.

Rodgers, G. K. (1987). Time of onset of full thermal stratification in Lake Ontario in relation to lake temperature in winter. Canadian Journal of Fisheries and Aquatic Sciences 44: 2225-2229.

Ruberg, S. A., Vanderploeg, H. A., Cavaletto, J. F., Lang, G. A., Liebig, J. R., Miller, T. C. and Agy, M. (2001) Plankton survey system. Proceedings of the Oceans 2001 MTS/IEEE Conference, Honolulu, HI, November 5–8, 2001 Marine Technology Society, Washington, D.C. pp. 1899-1903

Saiz, E., Rodriguez, V. and Alcaraz, M. (1992). Spatial distribution and feeding rates of Centropages typicus in relation to frontal hydrographic structures in the Catalan Sea (West- ern Mediterranean). Marine Biology 112:49-56.

Spain, J.D., Wernert, C.M. and Hubbard, D.W. (2015). The structure of the spring thermal bar in Lake Superior. J. Great Lakes Res., 2(2):296-306.

Scavia, D. and Bennett, J. R. (1980). Spring transition period in Lake Ontario--A numerical study of the causes of the large biological and chemical gradients. Canadian Journal of Fisheries and Aquatic Sciences 37:823-833.

Scavia, D. and Fahnenstiel, G. L. (1987). Dynamics of Lake Michigan phytoplankton: mechanisms controlling epilimnetic communities. J. Great Lakes Res. 13: 103-120.

Selgeby, J.H. (1975). Life histories and abundance of crustacean zooplankton in the outlet of Lake Superior, 1971-1972. J. Fish. Res. Board Can. 32:461-470.

Stoermer, E. F. (1968). Nearshore phytoplankton populations in the Grand Haven, Michigan vicinity during thermal bar conditions. Proc. 11th Conf. Great Lakes Res. 137-150.

Torke, B.G. (1975). The population dynamics and life histories of crustacean zooplankton at a deep-water station in Lake Michigan. Ph.D. Thesis, University of Wisconsin, Madison. 91pp.

Torke, B.G. (2001). The distribution of calanoid copepods in the plankton of Wisconsin Lakes. Hydrobiologia 453/454:351-365.

Tsydenov, B. O. (2019). Simulating phytoplankton growth during the spring thermal bar in a deep lake. Journal of Marine Systems 195 38–49.

Ullman, D., Brown, J., Cornillon, P. and Mavor, T. (1998). Surface temperature fronts in the Great Lakes. J. Great Lakes Res. 24:753–775.Vanderploeg, H. A., Johengen, T. H., Lavrentyev, P. J., Chen, C., Lang, G. A., Agy, M. A., Bundy, M. H., Cavaletto, J. F., Eadie, B. J., Liebig, J. R., Miller, G. S., Ruberg, S. A., McCormick, M. J. (2007). Anatomy of the recurrent coastal sediment plume in Lake Michigan and its impacts on light climate, nutrients, and plankton. J. Geophys. Res. Oceans 112. http:// dx.doi.org/10.1029/2004JC002379 (C03S90).

Vanderploeg, H. A., Liebig, J. R., Nalepa, T.F., Fahnenstiel, G. L., Pothoven, S. A. (2010). Dreissena and the disappearance of the spring phytoplankton bloom in Lake Michigan. J. Great Lakes Res. 36 (Suppl. 3), 50–59.c

Vanderploeg, H. A., Pothoven, S. A., Fahnenstiel, G. L., Cavaletto, J. F., Liebig, J. R., Stow, C. A., Nalepa, T. F., Madenjian, C. P. and Bunnell, D. B. (2012). Seasonal zooplankton dynamics in Lake Michigan: disentangling impacts of resource limitation, ecosystem engineering, and predation during a critical ecosystem transition. J. Great Lakes Res. 38, 336–352. http://dx.doi.org/10.1016/j.jglr.2012.02.005.

Vanderploeg, H. A., Pothoven, S. A., Krueger, D. Mason, D. M., Liebig, J. R., Cavaletto, J.F., Ruberg, S. A., Lang, G.A. and Ptáčníková, R. (2015). Spatial and predatory interactions of visually preying nonindigenous zooplankton and fish in Lake Michigan during midsummer. J. Great Lakes Res. 41 pp. 125-142.

Wang, Yutta. (2013). Lake Michigan Hydrodynamics: Mysis and Larval Fish Interactions. Theses and Dissertations. 381. https://dc.uwm.edu/etd/381.

Wilson, M. S. and Yeatman, H. C. (1959). Free-living copepoda. In Freshwater Biology, 2nd ed. Edited by W.T. Edmondson. John Wiley and Sons, New York. pp. 735-861.